Characterization and modeling source levels of commercial vessels in the Gulf of Mexico

Katrina H. Johnson [ID] ; Vanessa M. ZoBell [ID] ; Lynne E. W. Hodge; Melissa S. Soldevilla [ID] ;
John A. Hildebrand [ID] ; Kaitlin E. Frasier [ID]

Check for updates

View Online   Export Citation

07 December 2025 19:27:13

ASA
ACOUSTICAL SOCIETY
OF AMERICA

Characterization and modeling source levels of commercial vessels in the Gulf of Mexico

Katrina H. Johnson,[1,a)] ID Vanessa M. ZoBell,[1] ID Lynne E. W. Hodge,[2,3] Melissa S. Soldevilla,[2] ID John A. Hildebrand,[1] ID and Kaitlin E. Frasier[1] ID

[1]*Scripps Institution of Oceanography, University of California, San Diego, La Jolla, California 92037, USA*

[2]*Southeast Fisheries Science Center, National Oceanic and Atmospheric Administration, 75 Virginia Beach Drive, Miami, Florida 33143, USA*

[3]*University Corporation for Atmospheric Research's (UCAR) Cooperative Programs for the Advancement of Earth System Science (CPAESS), 3090 Center Green Drive, Boulder, Colorado 80301, USA*

ABSTRACT:

The Gulf of Mexico is among the noisiest marine regions globally, primarily due to widespread seismic airgun operations and vessel traffic. While airguns dominate the low-frequency soundscape, vessel traffic also contributes substantial high-amplitude noise in the same range low-frequency band (<500 Hz). Between August 2020 and July 2022, two underwater acoustic recording stations documented 13 930 vessel transits from five major ship types operating within commercial shipping lanes. Tankers and cargo ships were the most common, followed by tug-tows, passenger ships, and special crafts. Cargo ships and tankers had average broadband (20–1000 Hz) monopole source levels (MSLs) of ~183 dB re 1 μPa m, while tug-tows were 2–3 dB lower, and passenger ships/special craft were 4–5 dB lower. To investigate factors influencing low-frequency sound production, this study analyzed the relationship between vessel MSLs and ship characteristics, transit conditions, and oceanographic parameters. For this study, machine-learning models were trained to predict MSLs and their performance was compared to that of generalized additive models. Vessel speed was the most influential predictor, with additional contributions from deadweight, gross tonnage, length, and environmental parameters. This machine learning approach provides a tool to estimate MSLs in other regions and simulate the effects of noise reduction solutions, such as speed reduction or vessel design modifications.

I. INTRODUCTION

The Gulf of Mexico (GOM) is one of Earth's most anthropogenically impacted marine regions. Each year, over 100 000 cargo vessels transit to one of ten major ports in both the U.S. and Mexican GOM. Additionally, more than 3 $\times$ 10^9 barrels of petroleum products are exported annually from the Gulf Coast via tankers (EIA, 2024). These vessels produce low-frequency (<500 Hz) noise, generated primarily by propeller cavitation, which can travel hundreds to thousands of kilometers underwater in the deep ocean sound channel (Wilcock *et al.*, 2014).

Underwater radiated noise (URN), the acoustic energy radiated by individual vessels, varies with ship type, operating conditions (speed, deadweight, draft), and environmental factors (wind, current), and remains a challenge to accurately predict (McKenna *et al.*, 2013; Chion *et al.*, 2019; MacGillivray *et al.*, 2019). URN can vary substantially even within the same vessel class, making the estimation of URN for any individual vessel a complex process

(Chion *et al.*, 2019). Recent studies have highlighted current models for estimating ship noise often do not capture this variability effectively. For instance, Karasalo *et al.* (2017) found that predictions of existing URN models varied widely, and some underestimated the noise radiated from individual ships by as much as 20 dB. Similarly, Gassmann *et al.* (2017b) demonstrated that ship monopole source levels (MSLs) can vary by up to 10 dB for vessels of similar size and type at certain frequencies. These findings highlight the complexity of accurately modeling URNs from ships and underscore the need for continued refinement of prediction methods.

Although ship noise has been studied extensively along the U.S. West Coast and East Coast (Andrew *et al.*, 2002; McDonald *et al.*, 2006; Chapman and Price, 2011; McKenna *et al.*, 2012; McKenna *et al.*, 2013; Miksis-Olds and Nichols 2016), there has been little research on ship noise and noise mitigation in the GOM (Haver *et al.*, 2021). Compared to other U.S. coastal regions, the GOM features a unique vessel composition, with notably higher proportions of tankers. Tankers and cargo ships transit in designated shipping lanes designed to provide safe passage around oil

---

a)Email: kaj007@ucsd.edu

well structures (U.S. Department of Commerce, National Oceanic and Atmospheric Administration, National Ocean Service, 2024). Two major shipping lanes serve the Port of Galveston (GA) and the Port of South Louisiana (SL). The Port of GA handles more than 4×10^6 tonnes of cargo annually (Port of Galveston, 2024). Just north of the Port of GA is the Port of Houston, which is the largest importer and exporter of petroleum and petroleum products in the United States (Texas Comptroller of Public Accounts, 2024). The Port of SL moves over 50% of all U.S. grain exports, with 12 000 deep draft cargo ships traveling annually to the lower Mississippi River, and is one of the top energy transfer ports in the U.S., with over 43% of U.S. oil and petroleum imports (Port of South Louisiana, 2024). The Louisiana Offshore Oil Platform (LOOP), located in the SL shipping lane, is the U.S.'s first and only deep-water port specifically designed for offloading ultra-large crude carriers (ULCCs) and very large crude carriers (VLCCs). These massive oil tankers require water depths of up to 85 ft, which most U.S. ports cannot accommodate (Louisiana Department of Transportation and Development, 2024). As a result of commercial shipping and additional sources of noise pollution in the region, such as seismic surveys and fishing activity, chronic noise levels in the GOM are among the highest in the world (Estabrook et al., 2016; Wiggins et al., 2016; Haver et al., 2018).

To investigate the URN of vessels within this region, we deployed two acoustic sensors within the shipping lanes of the Port of GA and the Port of SL. We describe the characteristics of close-transiting ships recorded over a 2-year period and estimate MSLs for each transit. To understand the influence of vessel operational conditions, design parameters, and environmental factors on MSL, we developed and compared machine-learning-based models and generalized additive models (GAMs) to predict cargo ship and tanker MSLs. The trained models were used to visualize relationships between these parameters and MSLs. Model accuracy was quantified and compared with predictions from an existing model (MacGillivray and de Jong, 2021).

This study fills critical data gaps for understudied ship types, such as tankers and tug-tows, and reveals that MSL is influenced by a diverse array of variables, not just vessel speed. In addition, this study uses machine learning algorithms to predict MSL values, a method that has not been used for ship noise prediction. Understanding these various elements is crucial for developing accurate noise models and implementing effective noise reduction strategies in important marine habitats like the GOM. Marine managers may need to consider this complexity when designing mitigation measures, such as vessel speed reduction programs or technical modifications, to optimize their impact on URN reduction.

II. METHODS

A. Acoustic recordings

We deployed two long-term mid-frequency acoustic recording packages (MARPs) in the northern GOM within two shipping lanes, GA and SL (depth 200–230 m) (see Fig. 1 and see Suppl. 1 in the supplementary material). MARPs, a variation of high-frequency acoustic recording packages (HARPs), are bottom-mounted instruments equipped with a hydrophone with a 20 kHz sampling rate that is tethered approximately 20 m above the seafloor (Wiggins and Hildebrand, 2007). MARP hydrophone electronics were calibrated at Scripps Institution of Oceanography, and similar full systems were calibrated at the U.S. Navy's Transducer Evaluation Center facility in San Diego, CA. MARP hydrophones are composed of six cylindrical transducers (Benthos AQ-1; Teledyne Benthos, North Falmouth, MA) and pre-amplifier electronics with a known sensitivity between 20 Hz and 10 kHz. At 63 Hz, the maximum received level at the hydrophone ranged from 152.8 to 152.9 dB re 1 μPa, with clip levels ranging between 165.7 and 165.9 dB re 1 μPa.

B. Ship passage information

Acoustic recordings from a variety of ship types, including cargo ships (carrying non-liquid cargo), tankers (carrying liquid cargo), tug-tows, fishing vessels, passenger vessels, and special crafts, including mobile offshore drilling units, offshore supply vessels, and research vessels, were collected opportunistically from transits to and from the Port of SL and Port of GA from August 2020 to July 2022 (see Suppl. 1 in the supplementary material). We combined long-term acoustic recordings with synchronous Automatic Identification System (AIS) data from Marine Cadastre (Bureau of Ocean Energy Management and National Oceanic and Atmospheric Administration, 2023) and MarineTraffic (MarineTraffic, 2023) to create a database of vessel characteristics and MSLs. The AIS data consisted of the position of the vessel (latitude, longitude), as well as the Maritime Mobile Service Identity (MMSI) information, speed over ground (SOG), course over ground (COG), vessel type (tanker, cargo, etc.), length, width, and draft. Each vessel passage was treated as an independent event, but vessel identification was included as a predictor variable to assess whether specific vessels were louder than others. Design information incorporated from MarineTraffic included detailed vessel type (chemical/oil products tanker, bulk carrier, etc.), year built, maximum draft, minimum draft, shipbuilder, engine builder, maximum gross tonnage, maximum deadweight, and commercial size class. While we had access to maximum load metrics, operational load data were unavailable for this study. This limitation prevented us from directly testing hypotheses related to the impact of varying operational loads on vessel noise emissions, which likely affects both draft (for propagation modeling) and noise output.

The accuracy of draft measurements provided in AIS varies. In the Marine Cadastre dataset used for this study, the draft field represents maximum static draft, which is often greater than operational draft (ZoBell et al., 2021; Ainslie et al., 2022; Meyers et al., 2022). Moreover, the draft field was often unchanged between transits, suggesting that the measurement may not be routinely updated. An initial analysis using the maximum draft led to an

J. Acoust. Soc. Am. **158** (3), September 2025
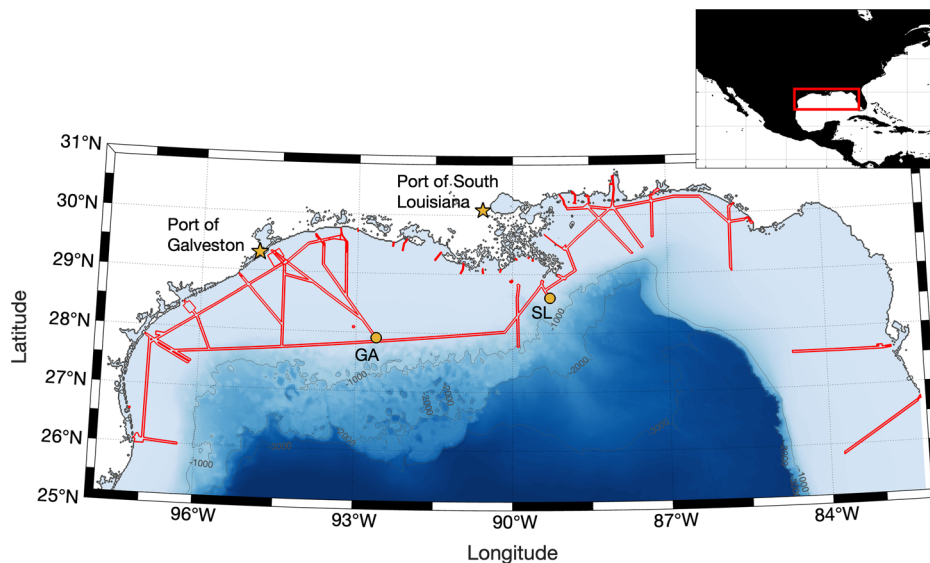
Johnson et al. 2251

FIG. 1. Map of the Gulf of Mexico passive acoustic monitoring locations (orange circles), Ports of Galveston (GA) and South Louisiana (SL) (orange stars), and location of shipping fairways (red lines). Bathymetric contours are shown for the 1000 and 2000 m contours.

underestimation of the Lloyd's mirror effect and an underestimation of vessel noise at low frequencies. To correct this, we implemented a method that analyzes the characteristic influence of Lloyd's mirror interference within the measured sound spectrum of each ship passage to estimate vessel draft directly from the acoustic recordings (Gassmann *et al.*, 2017b). Lloyd's mirror arises when sound from a near-surface source travels both directly to an underwater hydrophone and via a reflection at the sea surface, resulting in destructive interference in the recorded spectrum. The frequencies affected are related to the source's depth, typically assumed to be the top of the propeller, with deeper source depths causing longer wavelengths to be out of phase. For each ship passage, we smoothed the spectrum from 10 to 200 Hz, using a 20 Hz moving average. We then identified the highest-amplitude local maximum in the smoothed range and considered this to mark the spectral "roll-off" frequency. This frequency is indicative of the point at which destructive interference begins. We then constructed a lookup table by simulating theoretical transmission loss curves for a range of possible source depths from 1 to 25 m in 0.1 m increments using a Lloyd's mirror acoustic propagation model (Carey, 2009; Audoly and Meyer 2017; Gassmann *et al.*, 2017b). These modeled curves incorporated the vessel's slant range, hydrophone depth, and the measured local sound speed. For each source depth, we determined the frequency at which the modeled Lloyd's mirror transmission loss intersected and fell below the prediction from a simple spherical spreading model (Gassmann *et al.*, 2017b). The frequencies of these crossings were compared to the empirically observed roll-off frequency from the data. The best-fit source depth was identified as the one whose simulated crossover frequency most closely matched the observed roll-off frequency, yielding an objective, automated estimate of the vessel's acoustic source depth. This estimated source depth, assumed to be the top of the propeller, was then converted to an estimated draft for the vessel (see Suppl. 2 in the supplemental material).

To exclude distant transits with noise levels potentially affected by an overestimation of propagation loss at low frequencies and to mitigate potential effects of seabed reflections, we performed a linear regression analysis, which led us to apply a maximum closest-point-of-approach (CPA) cutoff of 700 m. We selected the 700-m CPA cutoff following a preliminary analysis evaluating broadband MSL dependence on CPA (see Suppl. 3 in the supplementary material). Broadband MSL decreased with increasing CPA, and 700 m was the greatest distance where broadband MSLs were unaffected. Bottom type and estimated bottom loss at our measurement sites were not used or calculated in the given context of deep water (>200 m) [ISO 17208-2; see ISO (2019)] and the 700 m CPA cutoff. However, it is important to note that bottom type and associated losses can influence sound propagation in shallow water environments, potentially affecting MSL estimates, especially at longer ranges or lower frequencies.

A total of 13 930 ship transits with paired acoustic and AIS data were recorded within 700 m of the two MARPs, and their associated vessel design data were documented. For a case study to examine whether detailed ship design information could improve model accuracy, we extracted nine parameters, including detailed vessel type, year built, maximum draft, minimum draft, shipbuilder, engine builder, maximum gross tonnage, maximum deadweight, and commercial size class manually from MarineTraffic for the 3670 ships that traveled within one horizontal water depth (200 m) of the MARP (see Sec. II F and see Suppl. 4 in the supplementary material for additional details). We confirmed that these vessels were representative of the full sample of transiting vessels by comparing the distributions of operational and ship design metrics between the case study and full datasets.

C. Acoustic data quality control

To avoid contamination of ship transits with high levels of background noise from non-target noise sources, we truncated our predicted spectra at 20 Hz to avoid the influence of

low-frequency hydrophone cable strumming caused by subsurface ocean currents. Similarly, we excluded periods with high airgun noise levels from the MSL analyses by excluding days where the mean amplitude at 40 Hz, a representative band for airguns, exceeded 100 dB re 1 μPa m (Wiggins *et al.*, 2016; Frasier *et al.*, 2023). Truncating our analysis frequency at 20 Hz may have resulted in missing energy contributions from the primary propeller cavitation blade lines of vessels, which typically occur around 5–10 Hz (Jenson, 2001; Vorus, 2001).

D. MSL calculations

We estimated MSLs at the CPA of the vessel to the MARP using the Lloyd's mirror propagation loss model described in detail in Gassmann *et al.* (2017b) and ISO (2019). The data window period of each transit was determined by the time it took the vessel to transit its length. Each vessel transit acoustic recording was divided into 1-s segments. A 50% overlap between adjacent segments and a Hanning window with a length equal to the sampling frequency was applied to each segment to reduce spectral leakage and enhance temporal resolution while maintaining 1-s analysis intervals. The analysis utilized a 20 000-point fast Fourier transform (FFT). This configuration produced a time-frequency representation with temporal and spectral resolutions of 1 s and 1 Hz, respectively. Third-octave level (TOL) bands were calculated by converting the 1 Hz binned sound pressure levels (SPLs), which are measures of the pressure variation caused by a sound wave relative to a reference pressure, within each TOL band to linear space and then summing them and converting back to dB [Eq. (1)],

$$L_{\text{third-octave}} = 10 \log_{10}\left(\sum_i^1 10^{L_i/10}\right)_1 - 10 \log_{10}(\Delta f), \quad (1)$$

where i represents the index for each 1 Hz frequency bin within the specific TOL band being analyzed, L_i is the 1 Hz binned SPL, and Δf is the bandwidth of the TOL band in Hz. These values were adjusted for the bandwidth of each TOL band to achieve units of dB re 1 μPa^2/Hz.

We applied a propagation loss model that corrects for the Lloyd's mirror effect (N_{PL}) to the SPL to estimate MSL, accounting for reflections at the sea surface (ISO 17208-2:2019) [see (Eq. (2)]. The N_{PL} model ignores sound refraction in the water column and reflections with the seafloor and solely accounts for reflections from the sea surface (Audoly and Meyer 2017; Gassmann *et al.*, 2017b; ISO, 2019). The propagation loss of a near-surface sound source in deep water, considering the Lloyd's mirror effect, is given by

$$N_{\text{PL}} = -20 \log_{10}\left(r_0 \left| \frac{e^{jkr_1}}{r_1} - \frac{e^{jkr_2}}{r_2} \right|\right), \quad (2)$$

where r_1 is the distance from the source to the receiver, r_2 is the distance from the reflected image source to the receiver, r_0 is the reference distance (1 m), k is the wave number

($k = 2\pi f/c$, where f is the frequency of the wave and c is the speed of sound) in rad/m, e is Euler's number, and j is an imaginary unit in complex number representation. Source depth, used to determine r_2, was taken to be equal to 70% of the vessel draft, as stated in ISO 17208-2:2019 (ISO, 2019). Harmonic mean sound speeds were calculated from depth, temperature, and salinity data from the Global Ocean Forecasting System (GOFS) 3.1:41 depth layer model, incorporating global water column data in 1/12° spatial resolution (Naval Research Laboratory, 2014–2024). MSL in broadband and TOL bands were derived from the resultant MSL values in 1 Hz resolution. Broadband MSLs were calculated by converting the dB sound levels to a linear scale, numerically integrating the linear values over the desired frequency range (20 Hz–1000 Hz), and converting the integrated linear value back to dB re 1 μPa m.

E. Environmental data

Environmental data, including temperature, salinity, and current and surface wind direction and velocities in the east and west directions, were collected from the Hybrid Coordinate Ocean model (HYCOM) GOFS 3.1 Global Analysis (Naval Research Laboratory, 2014–2024). For each vessel's CPA, environmental variables were extracted at a temporal resolution of 3-hourly intervals. Depth-resolved variables were processed to compute sound speed profiles at each meter of depth. Near-surface currents (top 5 m layer) and wind velocities (10 m height) were used in hydrodynamic analyses, while sound speed calculations focused on the hydrophone deployment depth, derived by depth-averaging profiles around the MARP instrument's elevation. Environmental conditions were synchronized with CPA timestamps to match HYCOM's 3-hourly outputs, ensuring temporal alignment between ship passages and oceanographic variables. We used these data to investigate the effects of the environment on estimated ship MSLs, as we hypothesized that environmental factors may contribute to MSL variability.

The current and wind direction and speed were used to determine the magnitudes of the current and wind, as well as wind resistance. To calculate wind resistance, we considered wind directions ranging from 0° to 360°, where 0° represents wind coming directly head-on toward the vessel, and 180° represents wind blowing directly from behind the vessel. We then computed the relative wind velocity by decomposing both vessel and wind velocities into their east and north components. The relative velocity was determined by combining these components vectorially. We calculated the effective angle between the vessel and the wind using the relative velocity and the speeds of the vessel and wind. We then computed the wind resistance factor by squaring the relative velocity and multiplying it by a direction-dependent drag coefficient, which is typically ship-type-dependent (Frasier *et al.*, 2022). While we calculated wind resistance, current resistance was not computed because these calculations require detailed hull geometry data (e.g., wetted

J. Acoust. Soc. Am. **158** (3), September 2025

Johnson *et al.* 2253

surface area, drag coefficients) that were unavailable. Instead, we provided the neural network (NN) with current magnitude/direction and vessel operational parameters (COG, SOG) and design parameters (ship type), allowing it to infer current effects implicitly as the NN framework inherently captures interactions between variables. For example, a vessel traveling against a strong current may reduce speed or adjust course, indirectly altering its noise profile. The NN learns these nonlinear relationships directly from the raw current data (direction/speed) and vessel kinematics, eliminating the need for explicit hydrodynamic modeling.

F. Model frameworks

Cargo ships and tankers, accounting for 94% of the vessels recorded in this dataset, were further analyzed in the model training and development. To identify mechanisms to predict MSLs for cargo ships and tankers, we developed two modeling frameworks: NNs, which have not yet been used to predict MSL, and GAMs, which are a more common model type that has been used in underwater acoustics and MSL prediction (McKenna *et al.*, 2013; Jalkanen *et al.*, 2018; Piccolo *et al.*, 2019). When comparing the NN to the GAM, we focused on broadband MSL predictions, as GAMs are limited to single-output predictions. When comparing different NN configurations, TOL MSL was used to examine MSL estimates over a range of frequencies.

For each model type (NN or GAM), we trained three different models based on the data collected: Basic, Basic with HYCOM, and Full. The Basic model included information regarding the generic ship type, length (m), draft (m), SOG (kn), MMSI, and COG, information that is easily accessed from AIS data. The Basic with HYCOM model included the Basic data along with the current direction (degrees) and magnitude (m/s), and wind direction (degrees) and magnitude (m/s). The Full model included the Basic with HYCOM data along with the detailed vessel type, year built, maximum draft (m), minimum draft (m), shipbuilder, engine builder, width (m), maximum gross tonnage, maximum deadweight (tonnes), and commercial size class. For categorical variables (vessel type, MMSI, shipbuilder, engine builder, commercial size class), we applied label encoding, which assigns a unique integer to each category without implying any ordinal relationship. This allowed us to transform all qualitative variables into numerical values suitable for input into our models. Each variable was then normalized by subtracting the mean and dividing by the standard deviation (SD) computed across the entire dataset. Circular statistics were applied to directional variables where appropriate, specifically wind direction, current direction, and course over ground, which are measured on a $0°-360°$ scale. To address missing predictor values, we excluded any ship transit for which one or more predictor variables were missing. As a result, only transits with a full set of predictor data were included in the training and testing of the models.

We evaluated seven NN models and two GAM models to compare MSL predictions across different model frameworks and input data configurations. The NN models included configurations for both 700 m and 200 m distances: 700 m Basic, 700 m Basic with HYCOM, 200 m Basic, 200 m Basic with HYCOM, 200 m Full, 200 m Full Broadband, and 200 m Basic Broadband. All NN models used the same architecture but varied in input data. In contrast, GAMs focused exclusively on the 200 m distance with Basic and Full input datasets to provide a baseline comparison to the NN framework. The Broadband NN model was specifically designed to predict broadband MSL for direct comparison with the GAMs.

Basic and Basic with HYCOM models were developed on all available data (vessels with CPA within 700 m), while the Full model was developed only on case study data (vessels within 200 m). This approach allowed us to thoroughly explore the capabilities of NNs across various configurations while ensuring a fair comparison to GAMs in terms of predictive accuracy and input features.

G. Model implementations

Our NN model frameworks were informed by prior examples from the marine acoustics machine learning literature (Wang *et al.*, 2021; Walker *et al.*, 2024; Liu *et al.*, 2025). We trained the networks in MATLAB 2023a (MathWorks, 2023) using the Deep Learning Toolbox to predict ship MSLs. The majority of the data, 60%, were allocated to training to provide the NN with sufficient examples to learn patterns and relationships between input variables and MSL predictions. Our validation set was approximately 10% of the data and was used for hyperparameter tuning and monitoring model performance during training. This ensured that the model did not overfit the training data and allowed for adjustments to improve generalization. Our testing dataset was 30% of the data to evaluate the final model's performance on unseen data. This split ensures that the test results are representative of real-world scenarios where the model encounters new vessels or environmental conditions.

For NN model selection and fitting, we tested multiple combinations of hyperparameters, including the number of layers, neurons per layer, learning rate, and dropout rate. Deep networks capture nonlinear ship noise patterns better than shallow architectures (Wang *et al.*, 2021; Liu *et al.*, 2025). The final architecture was selected based on the lowest root mean square error (RMSE). We employed the RMSprop optimizer, chosen for its adaptive learning rate capabilities in spectral regression tasks (Tieleman and Hinton, 2012). The batch size was set to 50, meaning that the network processed 50 samples at once, which balances computational efficiency with generalization ability. The network consisted of an input layer of varying numbers of input nodes (each node representing one predictor variable) and five fully connected hidden layers because this balances model capacity and computational efficiency for spectral

regression tasks. We used 100 nodes per layer because that has been empirically determined to optimize performance without overfitting for a dataset of this size (Benkendorf and Hawkins, 2020). We used hyperbolic tangent activation functions for all hidden layers and a linear activation function for the output layer, which is typical for regression models. We used three dropout layers to reduce overfitting (Lin *et al.*, 2023) and 18 output nodes, which matches the number of TOL bands (20–1000 Hz), or 1 output node, which matches the broadband MSL output. A maximum of 200 epochs were allowed for each network, with a validation frequency of 100 and patience of 5, which halted training when validation loss stopped improving to minimize the risk of overtraining.

To compare the NN framework to a more widely used model, we created GAMs in R version 4.3.3 using the R software package *mgcv*, with a Gaussian family and identity link function to predict broadband MSL (Hastie and Tibshirani, 1986; Wood, 2017; R Core Team, 2024). All predictor variables were included as additive terms with smoothing splines for continuous variables and as factors for categorical variables. SOG, width, length, and draft were found to be linear terms, so we included them as linear variables instead of smoothed variables. We specified $k = 4$ as the spline basis dimension, representing the number of basis functions used to model the smooth terms in the GAM, to minimize the risk of overfitting (Wood, 2017). For GAM selection and fitting, we initially included all variables in the model and then used a backward stepwise approach, removing terms with p values of >0.05. Smooth terms were kept if their estimated degrees of freedom were significantly different from zero. We intentionally used the same predictor variables in both the GAM and NN models, rather than optimizing the GAM via the Akaike information criterion (AIC), to ensure a direct comparison of model performance without confounding differences in input variables.

To ensure comparability between the NN and GAM frameworks, we deliberately included the same set of predictors in both models, even if some variables were collinear. This decision was made to isolate differences in model performance and predictive capabilities, rather than differences in input features. We compared NN and GAM performance using RMSE and R^2. MSL data from TOL bands were used when comparing NNs to each other, while broadband (20 Hz–1000 Hz) MSLs were used when comparing NNs to GAMs. We used a separate NN for broadband MSL because summing predicted TOLs can compound errors from each band, reducing accuracy. Directly predicting broadband MSL allows for better optimization and avoids error propagation. This approach also ensures a fair comparison between models, as predicting a single value differs computationally from predicting multiple TOLs.

H. Model evaluation

We evaluated nine models (seven NNs and two GAMs) to compare MSL predictions between model frameworks

and the amount of data supplied (Basic, Basic with HYCOM, Full). We used RMSE to compare predictions from each model with observations in the test data as

$$\text{RMSE} = \sqrt{\frac{1}{N}\sum_{n=1}^{N}\left(y_n - \widehat{y_n}\right)^2}, \tag{3}$$

where N is the number of observations in the test dataset, y_n is the n-th observation in the test dataset, and $\widehat{y_n}$ is the model estimate of the observation. The values of y_n and $\widehat{y_n}$ can be a single value (broadband MSL) or multiple values (spectra of TOL MSLs). While the best-performing model was generally selected by minimizing RMSE [Eq. (3)], we recognized that RMSE strongly penalizes instances where differences between observations and model predictions are large. To address this limitation and gain a more comprehensive understanding of model performance, we considered three metrics: mean RMSE, median RMSE, and SD of RMSE. This approach allowed us to assess overall model accuracy (mean), identify typical performance unaffected by outliers (median), and understand the spread of prediction errors (standard deviation). By examining these metrics together, we could better interpret model performance, particularly in cases where a few large errors might disproportionately influence the mean RMSE, and identify models that performed consistently well across various conditions, rather than those that might have a low average error but high variability in performance.

We also compared our models to the Joint Monitoring Programme for Ambient Noise in the North Sea project (JOMOPANS) (MacGillivray and De Jong, 2021), a source level spectrum model based on AIS-derived parameters, including length, SOG, and type. The distinction between the models developed in this study, which include environmental, design, and AIS-derived parameters, and the JOMOPANS model allows us to evaluate how including additional data sources may improve MSL prediction accuracy and/or whether machine learning frameworks like NNs provide advantages over traditional approaches.

We analyzed the partial dependence plots generated by the GAM to gain insights into the relationships the model identified (Friedman, 2001; Greenwell *et al.*, 2018). To elucidate the relationships that the NNs learned, we created similar partial dependence visualizations by holding all variables constant except one (Greenwell *et al.*, 2018). For every transit, we manipulated the variable of interest (e.g., draft, length, SOG, etc.) using a range of values observed for the commercial ships. We then predicted the MSL based on the variables [Eq. (4)], which were plotted with confidence intervals to visualize the relationships the NN identified within the data. We calculated the effect size of each variable at 20, 63, 250, and 1000 Hz and broadband level as representative low, mid-, and high frequencies to quantify the predictor's importance in determining TOL MSL for each transit as

$$\eta = \frac{1}{N}\sum_{n=1}^{N}\left(\frac{(10^{\text{MSL}_n,\max/10}) - (10^{\text{MSL}_n,\min/10})}{(10^{\text{MSL}_n/10})}\right), \tag{4}$$

Johnson *et al.* 2255

where η represents the effect size, N is the total number of vessel transits, n represents the n-th vessel transit, $MSL_{n,max}$ and $MSL_{n,min}$ are the predicted mean square levels for the maximum and minimum values of the variable of interest for that transit, respectively, and MSL_n is the mean predicted value across the variable's range for that transit. This approach computes the effect size on a linear scale to avoid issues with logarithmic division. The magnitude of the effect size indicates the strength of the relationship (a larger magnitude effect size means a stronger relationship with MSL), while the sign indicates its direction (a positive or a negative relationship). A positive effect size means that as the predictor variable increases, the MSL increases, while a negative effect size means that as the predictor variable increases, the MSL decreases.

III. RESULTS

The dataset revealed distinct patterns in vessel composition, size, and MSLs influenced by key predictors such as speed over ground, deadweight, and vessel dimensions.

A. Measured variables

The vessel traffic within 200 m at sites GA and SL exhibited distinct patterns in vessel types while sharing similarities in operational and environmental conditions. Site GA was dominated by tanker traffic (63% of transits within 200 m), with 1184 transits from 942 unique vessels, followed by cargo ships with 683 transits from 597 unique vessels. In contrast, site SL had a higher prevalence of cargo ships (66% of transits within 200 m), recording 801 transits from 623 unique vessels, while tankers accounted for 404 transits from 303 unique vessels. Tug-tows emerged as the third most common vessel category at both sites, with 52 transits of 49 unique vessels at GA and 43 transits of 17 unique vessels at SL (see Suppl. 5 in the supplementary material). Additionally, passenger ships and special craft vessels were present in small numbers.

Despite these differences in vessel type distribution, the operational and design characteristics of ships were remarkably similar across both sites (Fig. 2 and see Suppl. 6 in the supplementary material). Vessel sizes ranged widely, with gross tonnage spanning from approximately 100 to 160 000 and lengths varying between about 50 and 350 m [Fig. 2(E)]. The majority of vessels fell within the 150–250 m length range, indicating a predominance of medium to large commercial vessels [Fig. 2(C)]. Vessel speeds showed a distribution from near stationary to about 20 kn, with a notable concentration between 10 and 15 kn [Fig. 2(A)]. This pattern suggests that ships commonly travel at these speeds within the shipping lanes in the region, though further data would be needed to determine if this trend is consistent across the wider Gulf area.

The age profile of the fleet was diverse, ranging from newly built vessels to those over 40 years old, with a median age of approximately 10–15 years [Fig. 2(F)]. This mix of newer and older vessels reflects the ongoing fleet renewal

process alongside the continued operation of older ships. Vessel drafts varied from 1.4 to 21.9 m, with most falling between 3 and 7 m, reflecting the different vessel types and their capacities [Fig. 2(D)].

The environmental data were comparable between sites (see Suppl. 6 in the supplementary material). Wind magnitude, current magnitude, and sound speed displayed some seasonal patterns. Wind speeds were typically greater in the winter compared to the summer [Fig. 3(A)]. Current speeds varied over time, with less clear trends but demonstrated some seasonality, with increased current speeds occurring in the fall [Fig. 3(C)]. Sound speeds, which are influenced by factors such as water temperature and salinity, displayed clear seasonal patterns, peaking during the summer months and having lower values in winter [Fig. 3(B)].

This similarity in operational and ship metrics and environmental conditions justified the combination of GA and SL data into a single database for subsequent analyses, enhancing the robustness of the dataset for modeling purposes. The integration of data from both sites provides a comprehensive representation of commercial vessel traffic in the region, capturing a diverse mix of vessel types that frequently transit these shipping lanes. This combined dataset not only increases the volume of data available for training models but also ensures a consistent set of input variables, allowing for a more nuanced characterization of MSLs associated with different vessel categories, operational conditions, and environmental factors.

Building upon our analysis of overall vessel characteristics, we examined the variability in MSLs across multiple transits of individual vessels. Data from two representative vessels, a container ship and a tanker, that transited frequently past the recording stations are presented to illustrate within-ship variability in MSLs across transits. Ship 1, a container ship, shows MSL variation of up to 15 dB across frequencies over 39 transits [Fig. 4(C)]. Similar patterns are seen across 26 transits of ship 2, an oil/chemical tanker [Fig. 4(D)]. The variability in MSLs across transits of the same ship indicates the importance of investigating operational and environmental parameters on MSL prediction.

The MSL estimates for major vessel categories were similar across the two monitoring sites (Table I), indicating that the modified Lloyd's mirror model effectively accounts for site-specific differences. The mean 63 Hz TOL MSL was comparable for cargo ships and tankers at 163–164 dB re 1 μPa m. In contrast, the 63 Hz TOL MSLs for tug-tows, passenger ships, and special craft vessels were 5–10 dB lower compared to those of cargo ships and tankers (Table I). The 63 Hz TOL MSLs of the remaining vessel categories displayed high variability, likely due to small sample sizes.

Examining the spectral shapes across vessel types reveals distinct characteristics. Cargo ships and tankers exhibit similar spectral patterns, with peak energy in the 10 Hz and a gradual decline at higher frequencies [Figs. 5(A) and 5(B)]. Their broadband (10–1000 Hz) source levels are also comparable, averaging around 184–185 dB re 1 μPa m. Tug-tows show a flatter spectrum with less pronounced low-frequency peaks,
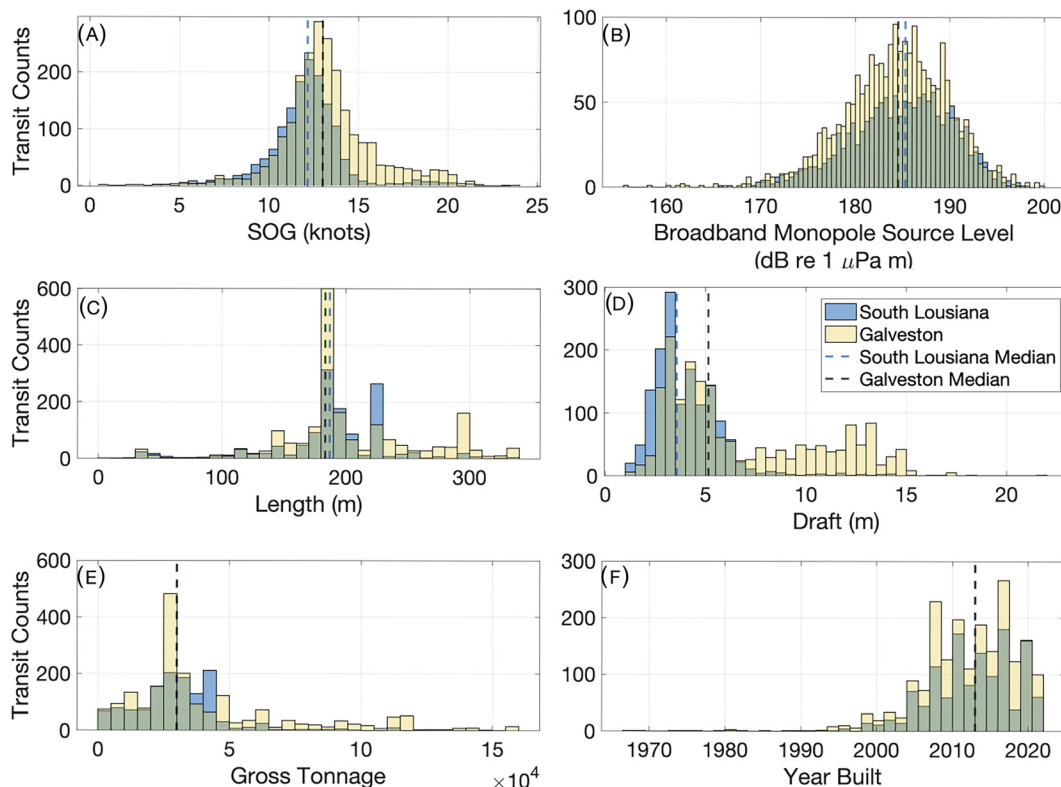
FIG. 2. Distributions of predictor and prediction variables within the dataset for all ship categories at the two recording locations, South Louisiana (blue bars) and Galveston (yellow bars). Broadband monopole source levels are computed over the 20 Hz–1000 Hz frequency range. Median lines for both gross tonnage (E) and year built (F) overlap, obscuring the South Louisiana line.

and their broadband levels are approximately 2–3 dB lower than those of cargo ships and tankers [Fig. 5(C)]. Special craft and passenger ships display more variable spectra, likely due to the smaller sample size, with broadband levels about 4–5 dB lower than the larger commercial vessels [Figs. 5(D) and 5(E)].

B. Model predictions and evaluations

We developed seven variations of NN models and two GAMs. The basic NN (700 m radius) performed the poorest, with a median root mean square error (RMSE) of 4.1 dB re 1 μPa m and a SD of 2.0 dB (Table II). The Basic NN (200 m radius), Basic NN with HYCOM (200 m radius), and Basic NN with HYCOM (700 m radius) models all had a median RMSE between 3.8 and 4.0 dB re 1 μPa m, with SDs of between 1.9 and 2.1 (Table II and Fig. 6). The full NN model (200 m radius) achieved a lower median RMSE of 3.0 dB re 1 μPa m with a SD of 1.3 dB (Table II and Fig. 6). Detailed ship design information did improve model accuracy, so we selected the full NN as the highest-performing model for predicting ship TOL MSL and utilized it in further analysis.

The highest-amplitude noise produced by ships typically occurs at frequencies below 20 Hz. However, we were unable to model this range because seismic airgun noise dominates the soundscape at these low frequencies, making ship noise prediction difficult. It is known from prior studies that ship noise is highest at the lowest frequencies (Ross, 1976; Gray and Greeley, 1980; Arveson and

Vendittis, 2000; Hildebrand, 2009), but we could not accurately predict below 20 Hz because of airgun interference.

The Basic NN and GAM models show median RMSE scores of 1.8 dB re 1 μPa m $\pm$ 2.0 dB and 3.2 dB re 1 μPa m $\pm$ 3.1 dB, respectively, while the Full NN and GAM models improve to 1.7 dB re 1 μPa m $\pm$ 1.9 dB and 2.9 dB re 1 μPa m $\pm$ 3.0 dB, respectively (Table III). These results suggest that NNs predict broadband MSLs more effectively than GAMs and incorporating more parameters slightly enhances model performance.

The results from the models allowed us to explore the relationships learned between the variables within the data. For the GAMs, we focused on the outputs of the full model (see Suppl. 7 and Suppl. 8 in the supplementary material) to maintain consistency with the NN approach and to provide a comprehensive view of potential influences on ship noise. Several predictors were identified as statistically significant ($p < 0.05$), including SOG, gross tonnage, deadweight, length, current magnitude, and wind magnitude (Fig. 7). Specifically, SOG and deadweight displayed strong positive trends with broadband MSL [Figs. 7(C) and 7(H)]. Environmental factors such as current and wind magnitude display a slight positive association, but the effect is weaker compared to deadweight and SOG [Figs. 7(D) and 7(E)]. Other variables, such as minimum draft, draft, width, year built, and direction of travel, showed non-significant p values ($p > 0.05$) (Fig. 7 and see Suppl. 7 and Suppl. 8 in the supplementary material). Cargo ships and tankers display no

J. Acoust. Soc. Am. **158** (3), September 2025
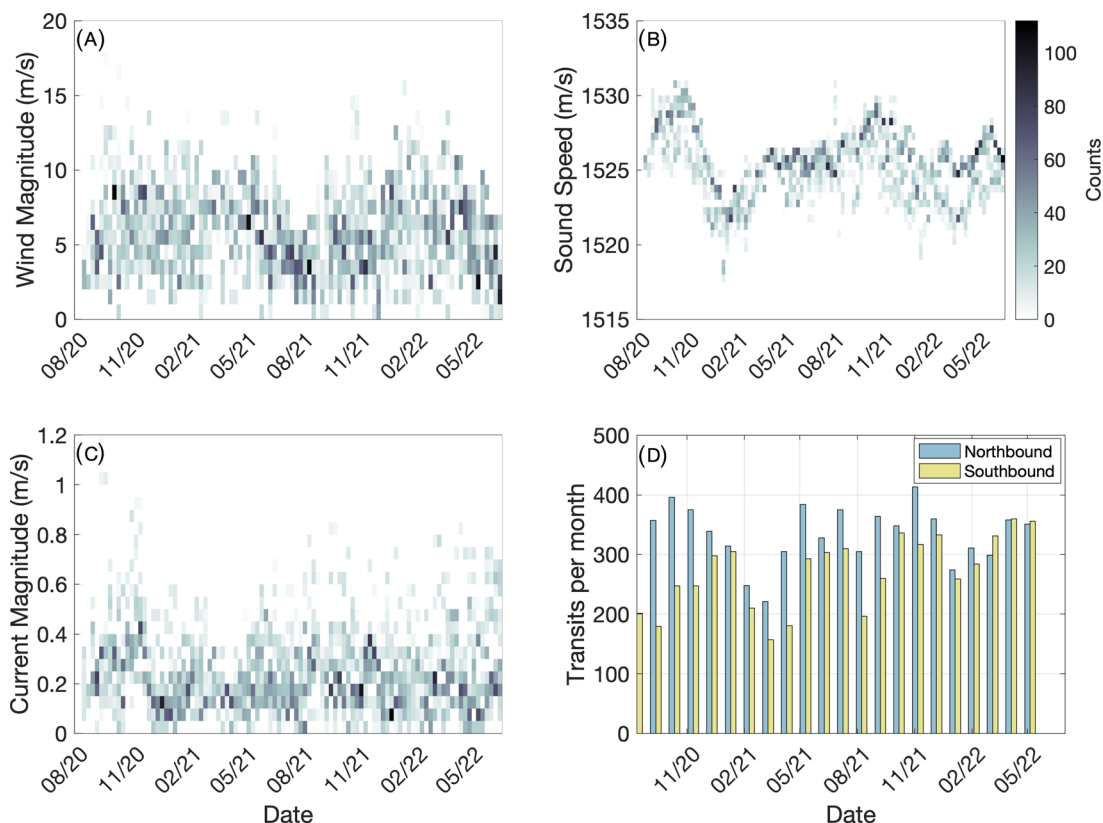
Johnson *et al.* 2257

FIG. 3. Temporal patterns in (A) wind magnitude (m/s), (B) sound speed (m/s), (C) current magnitude (m/s), with counts being the number of values at each sound speed and wind/current magnitude for each used in the models, and (D) ship transits per month at South Louisiana and Galveston from 2020 to 2022.
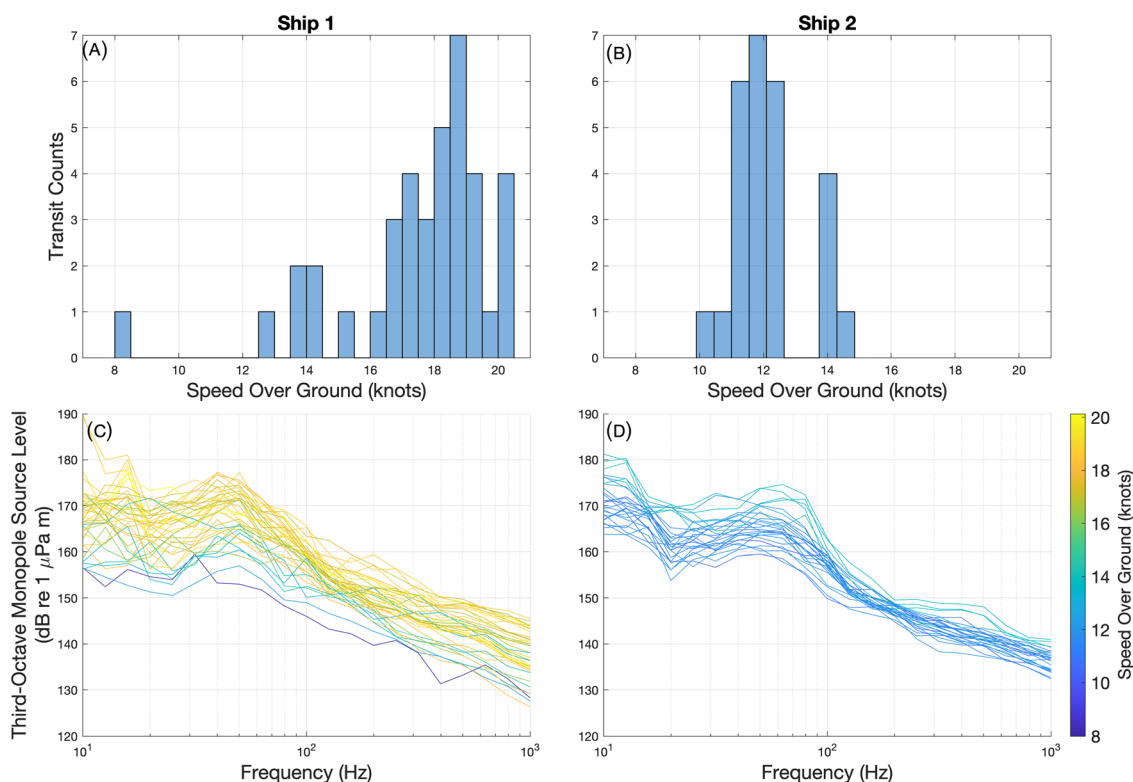

FIG. 4. Third-octave monopole source level variability for two representative ships with repeat transits in the dataset. (A) Distribution of speed over ground for 39 transits of ship 1, a container ship. (B) Distribution of speed over ground for 26 transits of ship 2, an oil/chemical tanker. (C) Third-octave monopole source level measurements of ship 1. (D) Third-octave monopole source level measurements of ship 2.

TABLE I. Numerical ship variables observed across ship types for ships detected within 200 m of either of the passive acoustic mooring sites. Large SDs occur in some cases when parameter distributions are not normal. Minimum and maximum values are provided as an alternative metric.

Parameter	Mean ± SD [minimum, maximum] for ship type				
	Tanker ($n = 1483$)	Cargo ($n = 1586$)	Tug-tow ($n = 95$)	Special craft ($n = 41$)	Passenger ($n = 40$)
Length (m)	197.4 ± 45.1 [94.7, 330]	204.9 ± 44.3 [64, 335.5]	64.5 ± 62.2 [25.3, 214]	118.0 ± 100.8 [35.5, 363]	310.2 ± 27.3 [219, 338.9]
Draft (m)	5.8 ± 3.6 [1.4, 18.3]	5.2 ± 3.0 [1.4, 21.9]	4.5 ± 2.1 [1.4, 10.3]	2.3 ± 1.3 [1.4, 7.8]	4.7 ± 2.6 [2.4, 13.9]
Speed over ground (kn)	12.9 ± 2.1 [4.1, 20.5]	12.8 ± 2.6 [2.1, 23.1]	10.6 ± 1.6 [5.9, 13.5]	12.1 ± 5.1 [0.8, 23.9]	16.8 ± 3.7 [7.3, 21.8]
Year built	2012 ± 6 [1976, 2022]	2011 ± 6 [1979, 2022]	2009 ± 8 [1967, 2018]	2003 ± 15 [1967, 2017]	2005 ± 6 [1991, 2016]
Max draft (m)	12.2 ± 1.7 [5.5, 21.5]	12.5 ± 2.0 [3.5, 18.5]	9.7 ± 1.7 [6.3, 13.9]	5.5 ± 2.2 [2, 14.4]	9.0 ± 0.9 [7.6, 11.8]
Min draft (m)	5.9 ± 1.2 [2, 9.5]	5.6 ± 1.0 [0.4, 8.5]	4.9 ± 1.3 [2, 8]	3.4 ± 1.2 [1, 8]	7.9 ± 1.0 [4.2, 8.8]
Width (m)	32.9 ± 7.3 [14.7, 60]	31.3 ± 5.2 [15.3, 48.4]	15.2 ± 7.2 [8.6, 32]	23.7 ± 20.4 [7.9, 76]	38.2 ± 3.7 [30.8, 49.1]
Gross tonnage	39 422 ± 29 450 [2897, 157 316]	35 649 ± 18 690 [2978, 96 816]	10 608 ± 583 [196, 2611]	3998 ± 7725 [323, 48 904]	126 230 ± 29 719 [53 015, 155 889]
Deadweight (tonnes)	53 492 ± 29 693 [3318, 296 681]	53 670 ± 24 579 [3950, 175 975]	995 ± 720 [26, 2366]	4223 ± 5037 [150, 26 332]	10 990 ± 2121 [6724, 13 815]
63 Hz mean MSL (dB re 1 μPa m ± dB)	163.5 ± 6.4 [137.8, 180.3]	164.1 ± 6.5 [131.1, 184.8]	159.8 ± 5.9 [146.1, 173.4]	157.5 ± 7.1 [138.7, 168.2]	158.2 ± 9.3 [135.2, 175.4]

difference in MSL prediction, nor do specific vessel types within these two categories of vessels [Figs. 7(K) and 7(L)].

Similarly, the final Full NN model reveals several key relationships between ship characteristics and predicted MSL across frequencies (20, 63, 250, and 1000 Hz) and broadband levels. SOG, gross tonnage, and deadweight demonstrate strong positive relationships with MSL across all frequencies and broadband levels, indicating that faster, heavier ships tend to be noisier [Figs. 8(B), 8(C), and 8(H)]. There appears to be no clear trend between the year a ship was built and predicted MSLs [Fig. 8(J)]. At broadband and 63 Hz, MSL shows a slight decrease as ship length increases [Fig. 8(F)]. Conversely, the 20, 250, and 1000 Hz frequencies are relatively stable with increasing ship length [Fig. 8(F)]. Draft and minimum draft show little to no discernible relationship with MSL [Figs. 8(A) and 8(G)]. Ship width at 20 Hz, 63 Hz, and broadband frequencies demonstrates a positive relationship with predicted MSL, suggesting that wider ships tend to exhibit higher noise levels in these ranges (Fig. 8I). In contrast, a slightly negative relationship is seen at both 250 and 1000 Hz frequencies, indicating a subtle decrease in MSL with increasing ship width in these specific frequency bands [Fig. 8(I)]. Both of the environmental predictors, wind and current magnitude, had small positive relationships with MSL across all frequencies and broadband levels [Figs. 8(D) and 8(E)].

Based on the effect size calculations, SOG, gross tonnage, and deadweight have the strongest positive effects on MSL at all frequencies (Fig. 9). Both current and wind magnitude display positive relationships with MSL (Fig. 9). Width has a positive effect on MSL at 20 and 63 Hz and at broadband frequency, but a negative effect on 250 and 1000 Hz, indicating that ship width may play a complicated role in MSL (Fig. 9). Ship length has a neutral or negative effect at all frequencies and broadband (Fig. 9). Draft, minimum draft, and year built have small mixed effects on MSL across all frequencies (Fig. 9).

Comparing the results of our GOM dataset processed through both the JOMOPANS model (MacGillivray and de Jong, 2021) and our GOM tanker and cargo-specific NN, we observed a median of the median difference of 3.5 dB, with the greatest difference at 20 Hz (9.9 dB) and the lowest difference at 200 Hz (0.1 dB). The JOMOPANS model had a median RMSE of 8.9 dB re 1 μPa m in calculating TOL MSL on our dataset (Fig. 10), while the NN developed in this study achieved a median error of 3.0 dB re 1 μPa m. This suggests that the JOMOPANS model may underestimate overall TOL MSLs compared to both the NN predictions and actual measurements, and highlights the performance of our region-specific models against the JOMOPANS model when applied to GOM data.

IV. DISCUSSION

This study underscores the importance of accurately estimating MSLs from commercial ships to model and mitigate their noise impacts on marine life and provides valuable first estimates of MSLs in the GOM. This advances our ability to assess and mitigate the underwater noise impacts from shipping across the GOM region and potentially in other regions.

By addressing previously understudied aspects of MSLs in the GOM, particularly for tankers and tug-tows, this work

J. Acoust. Soc. Am. **158** (3), September 2025
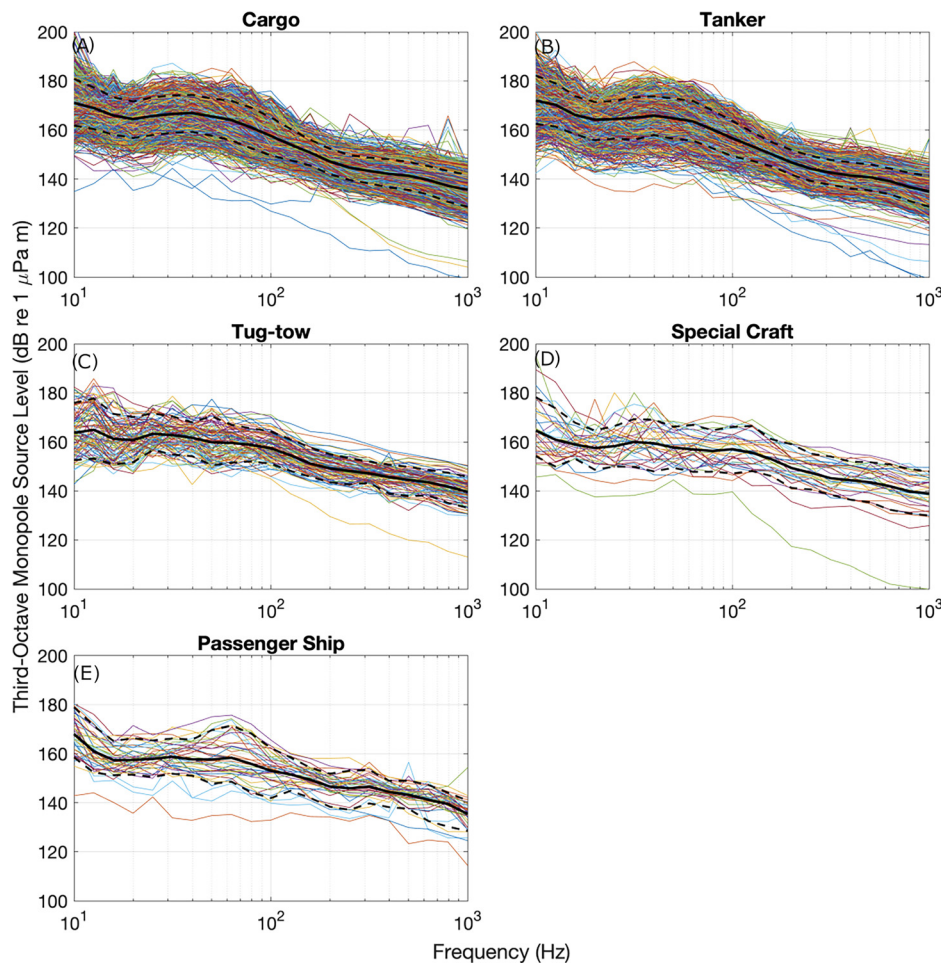
Johnson *et al.* 2259

07 December 2025 19:27:13

FIG. 5. Calculated third-octave monopole source level spectra corrected for bin width for all (A) cargo ($n = 1484$), (B) tanker ($n = 1588$), (C) tug-tow ($n = 95$), (D) special craft ($n = 41$), and (E) passenger ship ($n = 40$) transits in the 200 m dataset. A heavier black line indicates the mean, with dotted lines indicating the 10th and 90th percentiles.

offers valuable insights into these vessel categories. Tankers and cargo ships exhibited similar 63 Hz TOL MSLs, while other vessel types (tug-tows, passenger vessels, and special crafts) had 63 Hz TOL MSLs 5–10 dB lower than tankers and cargo ships across both sites (Table I). The prevalence of tankers and cargo ships in the studied shipping lanes highlights the importance of focusing noise management efforts on these large vessels. However, it is important to note that these findings are specific to designated shipping lanes and may not apply to smaller-scale noise management strategies implemented outside these areas. The similarity in TOL MSLs of tankers and cargo ships at the two monitoring locations allowed us to combine the

measurements into a single dataset, enhancing the robustness of the analysis and modeling and providing valuable insights for developing targeted noise management strategies in marine environments.

We demonstrated intra-vessel variability, which highlights the complex nature of MSL. The observed variability suggests that while vessel type and general characteristics are important predictors, there are additional factors at play, including operational conditions (e.g., speed, load, and propeller pitch), environmental factors (e.g., sea state and local oceanographic conditions), maintenance status (e.g., hull fouling, propeller condition), specific onboard machinery in use during the transit, and vessel design features not

TABLE II. Mean root mean square error (RMSE) scores for ten iterations of each neural network (NN). TOL monopole source levels for the Basic NN (200 m), Basic NN (700 m), Basic NN with HYCOM (200 m), Basic NN with HYCOM (700 m), and Full NN (200 m) were predicted as third-octave monopole source level spectra from 20 to 1000 Hz with mean and median units in dB re 1 μPa m and SD units in dB. Broadband monopole source levels for the Broadband Basic NN (200 m) and Broadband Full NN (200 m) were predicted as broadband monopole source level spectra from 20 to 1000 Hz with mean and median units in dB re 1 μPa m and standard deviation units in dB.

	RMSE for:						
Parameter	Basic NN (200 m)	Basic NN (700 m)	Broadband Basic NN (200 m)	Basic NN with HYCOM (200 m)	Basic NN with HYCOM (700 m)	Full NN (200 m)	Broadband full NN (200 m)
Mean	4.3	4.4	2.2	4.2	4.4	3.2	2.2
Median	3.9	4.1	1.8	3.8	4.0	3.0	1.7
SD	2.1	2.0	2.0	2.0	1.9	1.3	1.9

2260   J. Acoust. Soc. Am. **158** (3), September 2025
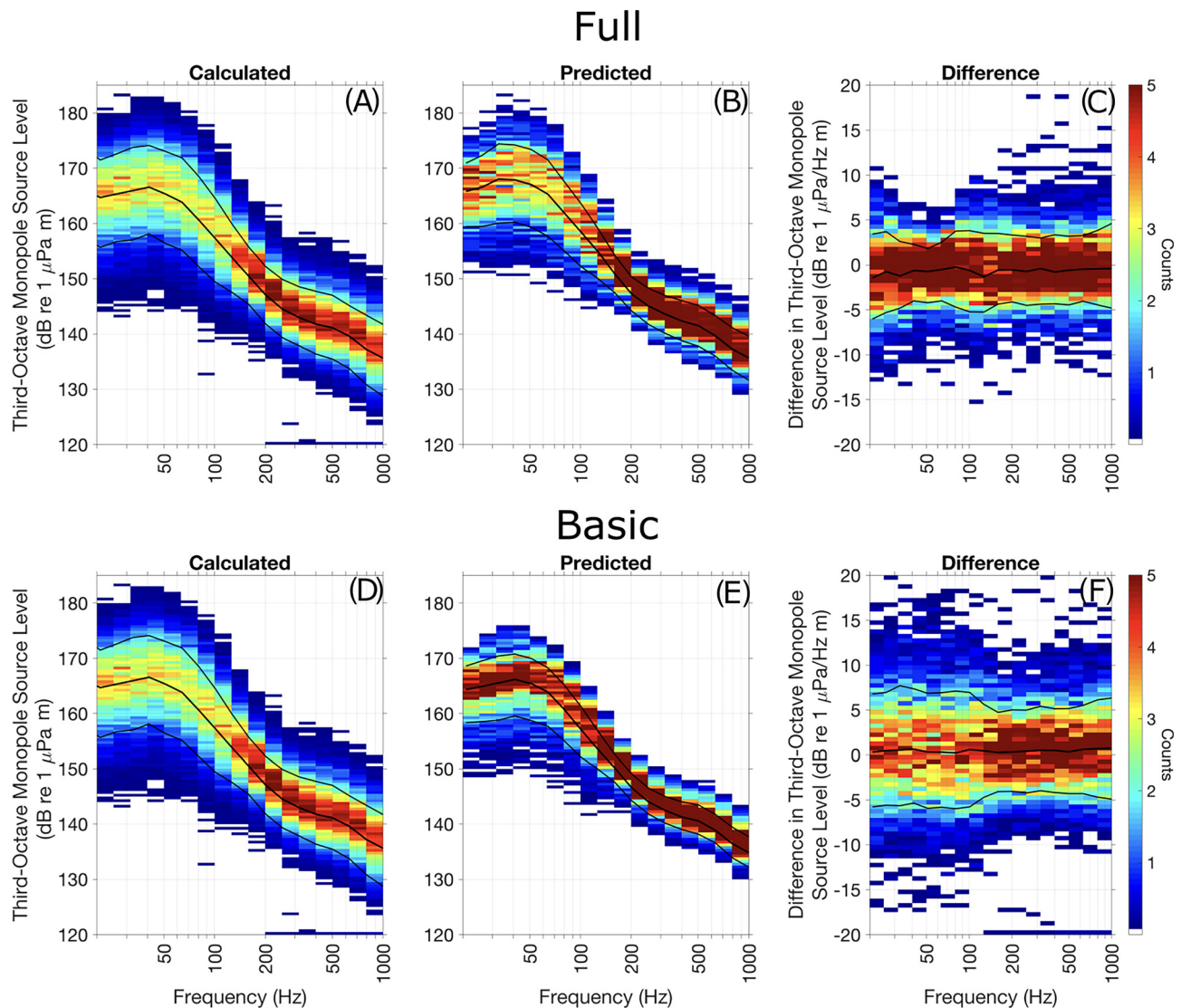
Johnson et al.

FIG. 6. (A) Calculated third-octave monopole source level spectra for the 200 m Full neural network model. The thicker black line indicates the median, while the lighter lines indicate the 10th and 90th percentiles. (B) Best predicted third-octave monopole source level spectra for the Full neural network model at 200 m. (C) Difference in third-octave monopole source level between the calculated (A) and model predicted (B) plots, computed as calculated − predicted. (D) Calculated third-octave monopole source level spectra for the 200 m Basic neural network model. (E) Best predicted third-octave monopole source level spectra for the Basic neural network model at 200 m. (F) Difference in third-octave monopole source level between the calculated (E) and predicted (F) plots.

captured by general characteristics (e.g., propeller design, hull shape) that can significantly influence a vessel's noise output on any given transit (Hildebrand, 2009; McKenna *et al.*, 2012; Leaper *et al.*, 2014; Veirs *et al.*, 2016).

TABLE III. Root mean square error (RMSE) scores for Full and Basic NN and GAM models (200 m). Monopole source levels were predicted in broadband from 20 Hz to 1000 Hz, with mean and median units in dB re 1 μPa m and SD units in dB.

	RMSE for:			
Parameter	Basic NN	Basic GAM	Full NN	Full GAM
Mean	2.2	3.8	2.2	3.6
Median	1.8	3.2	1.7	2.9
SD	2.0	3.1	1.9	3.0

Our analysis consistently identified speed as the primary explanatory variable driving variations in estimated MSLs, aligning with numerous studies (Putland *et al.*, 2018; Leaper, 2019; MacGillivray *et al.*, 2019; Burnham *et al.*, 2021; ZoBell *et al.*, 2023). The consistency across different modeling techniques underscores the robustness of this finding. This finding is supported by established physical principles, as higher vessel speeds increase propeller cavitation and turbulence, major contributors to ship noise (IMO, 2010; Gassmann *et al.*, 2017a; Leaper, 2019; IMO, 2023; ZoBell *et al.*, 2023). However, the relationship between speed and MSL is not uniform across all vessel categories, suggesting the influence of additional factors.

Our models reveal several other important relationships. Ship design parameters played a significant role, with

J. Acoust. Soc. Am. **158** (3), September 2025
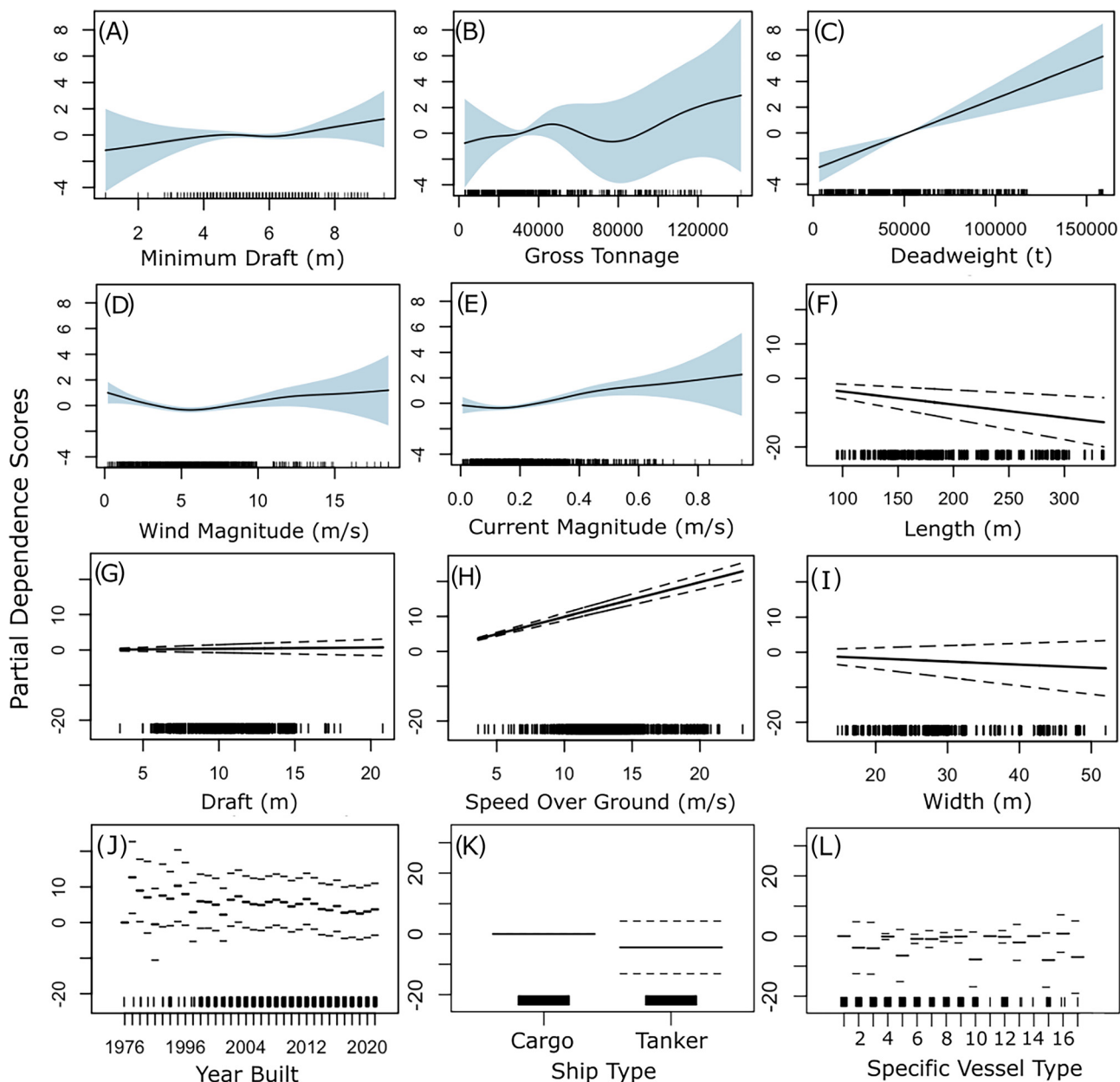
Johnson *et al.*   2261

FIG. 7. Partial dependence plots from the Full GAM showing mean (solid black line) and 95% confidence intervals (blue bands and dashed lines) of (A) minimum draft (m), (B) gross tonnage, (C) deadweight (tonnes), (D) wind magnitude (m/s), (E) current magnitude (m/s), (F) length (m), (G) draft (m), (H) speed over ground (kn), (I) width, (J) year built, (K) ship type, and (L) specific vessel type (1 = LPG tanker, 2 = general cargo, 3 = bulk carrier, 4 = oil/chemical tanker, 5 = container ship, 6 = crude oil tanker, 7 = asphalt/bitumen tanker, 8 = oil products tanker, 9 = chemical tanker, 10 = Ro-ro/vehicle carrier, 11 = special cargo, 12 = LNG tanker, 13 = special tanker, 14 = cement carrier, 15 = reefer, 16 = floating storage/production, 17 = heavy load carrier) (n = 998). The rug plot shows the distribution of the testing data.

factors related to vessel capacity, such as gross tonnage and deadweight, showing significant associations with MSL. Other metrics related to the vessel's submerged profile, like draft (operational, minimum, and maximum), appeared to have very little influence, indicating minimal residual influences of the Lloyd's mirror effect on MSLs. Within the combined commercial ship category (cargo ships and tankers) for modeling, there were no statistical differences in MSL, though we do note a difference in MSL by ship type if we expand to all vessel types seen in these commercial shipping lanes. The year built variable shows little to no effect on MSL at all frequencies. This pattern may imply that ship

age may not be relevant for noise emissions in the lower-frequency bands, where noise is often dominated by propeller cavitation and other low-frequency machinery sources.

While vessel characteristics such as SOG and deadweight emerged as the most influential predictors of MSL in our study, our results also indicate that environmental factors, specifically wind and current magnitude, play a measurable, although smaller, role. Both GAM and NN analyses identified wind and current magnitude as significant predictors, with MSL showing a slight positive association with both variables. However, the effect sizes for wind and current were consistently weaker than those observed for key
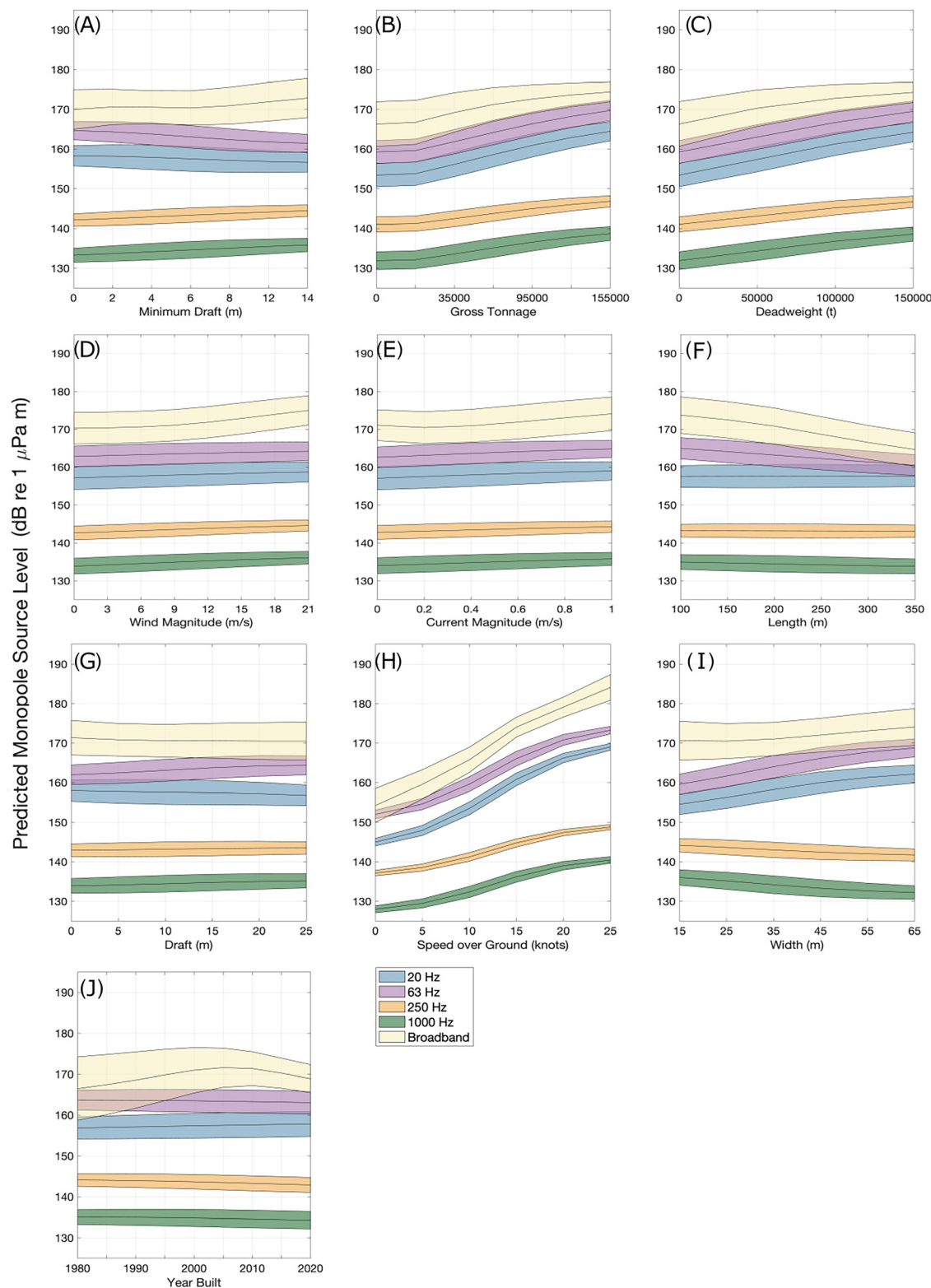
FIG. 8. Full neural network predictions of third-octave monopole source levels (dB re 1 μPa/Hz m) at 20, 63, 250, and 1000 Hz and broadband monopole source levels (dB re 1 μPa m) for cargo ships and tankers based on adjusting predictor parameters within the neural network ($n = 499$).

vessel attributes. The operational context of the Gulf region may partly explain this comparatively modest influence of environmental conditions. The presence of well-established shipping routes likely promotes consistent vessel behavior, potentially diminishing the relative impact of short-term or small-scale environmental fluctuations. Nonetheless, the statistical significance of wind and current magnitude in our models suggests that these factors should not be entirely discounted, particularly when considering specific scenarios or localized events. For instance, episodes of high winds or

J. Acoust. Soc. Am. **158** (3), September 2025
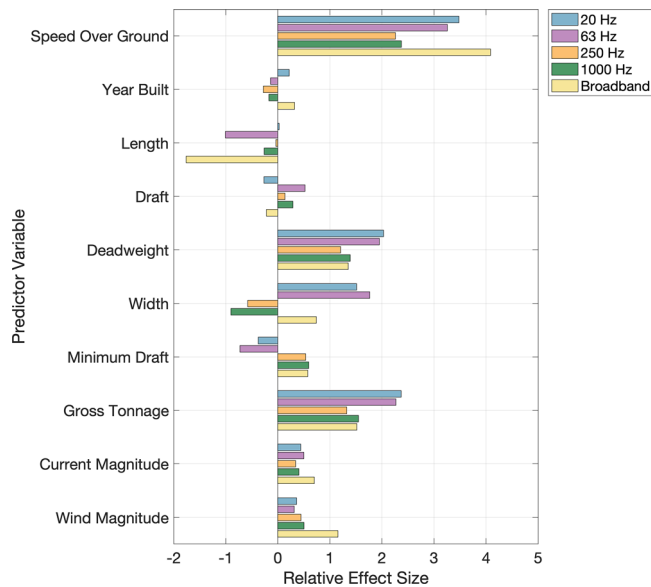
Johnson *et al.*   2263

FIG. 9. Relative effect size at 20, 63, 250, and 1000 Hz and broadband frequencies for combined cargo ships and tankers of all numerical predictor variables for the Full neural network model ($n = 499$).

strong currents may still affect individual vessel noise emissions (Hildebrand, 2009), even if such effects are not dominant in shaping overall patterns across the dataset. Thus, while vessel characteristics and operational conditions remain the primary drivers of underwater radiated noise in this context, environmental variables contribute additional nuance and should be considered in future efforts to model or mitigate ship noise, especially in regions or situations where environmental variability is greater.

The potential correlations and interactions among ship characteristics and operational parameters underscore the need for comprehensive modeling approaches that can account for multiple variables simultaneously (Fukushima, 1980; Silver *et al.*, 2017; Gao *et al.*, 2022). For example, vessel speed is a crucial factor influencing MSL, but its effects may vary, depending on other factors such as vessel size or load. Our findings highlight the importance of considering the core predictors, SOG, gross tonnage, deadweight, length, current magnitude, and wind magnitude, to accurately predict and mitigate URN from commercial vessels. The categorical variables, such as shipbuilder and engine builder, were included to capture vessel-specific effects that might not be explained by the main continuous predictors. These variables helped improve model predictions for vessels present in the training dataset, as they could account for unique characteristics or operational patterns associated with particular ships or manufacturers. However, their influence was limited when predicting noise levels for new vessels not previously seen by the model, as these categorical identifiers did not generalize beyond the training set. As a result, for broader applicability, the model relied more heavily on general ship characteristics like size and operational parameters. Additionally, variables like size class were largely incorporated by more granular predictors such as gross tonnage and deadweight, which provided a more detailed representation of vessel capacity and structure within the NN's nonlinear modeling framework which excels in implicitly learn complex relationships between interconnected variables, including nonlinear effects and interactions, without requiring explicit specification of these relationships in advance. This capability allows the model to capture nuanced dynamics, such as how speed-dependent noise output shifts with vessel load or design features, which are critical for developing effective mitigation strategies.

Our results show that the NN has better prediction accuracy compared to GAMs (Table III). The NNs stand out for their ability to predict multiple outputs simultaneously, allowing a single model to estimate MSL across various frequency levels in one step. GAMs have been used to estimate MSL at individual frequencies or bands (McKenna *et al.*, 2013), but typically require fitting separate models for each frequency of interest. While this is not a major impediment and does not prevent GAMs from being used for predicting spectra, the NN approach offers practical advantages in computational efficiency and workflow simplicity when predicting the full frequency distribution of MSL within a single unified framework. This capability is particularly valuable for assessing impacts on marine species with different frequency sensitivities (Szymanski *et al.*, 1999; Houser *et al.*, 2008; Peng *et al.*, 2015; Lucke *et al.*, 2016). Additionally, frequency-resolved predictions from NNs (and from GAMs, when applied at multiple bands) facilitate more detailed analyses of how propagation effects, such as frequency-dependent absorption, scattering, and boundary interactions, may shape observed noise patterns (Urick, 1983; Jensen *et al.*, 2011; Etter, 2018). While the NN itself does not explicitly model these propagation processes, frequency-resolved predictions can reveal patterns that are
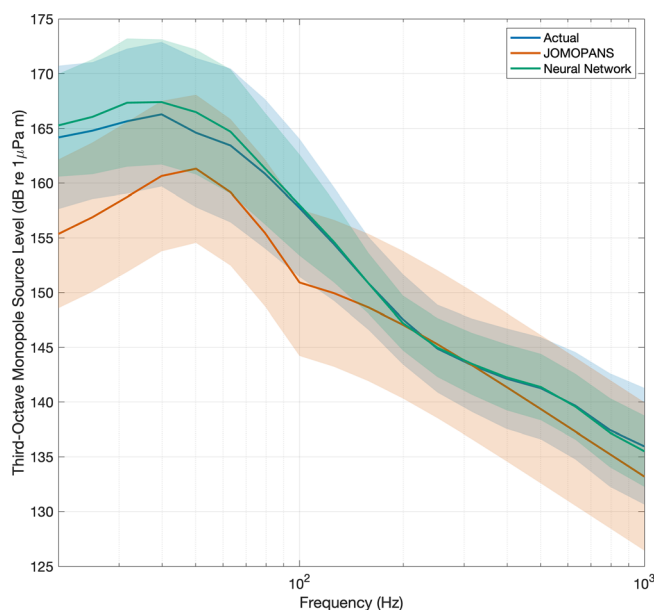

FIG. 10. Third-octave monopole source level comparison between the calculated (actual) values, the Full neural network predictions, and the Joint Monitoring Programme for Ambient Noise North Sea (JOMOPANS) model.

influenced by such effects, which may be masked in broad-band MSL analyses. Moreover, predicted MSL spectra can be directly integrated into propagation, ambient noise, or animal exposure models that target specific frequencies or bands, supporting comprehensive assessments of cumulative noise impacts. It is also important to note that GAMs can face substantial limitations when encountering new data that are outside the distribution of the training set. For example, if a ship was built in 1989 and the training data did not include any ships from that year, a GAM would not be able to make predictions for such out-of-sample cases. This inherent limitation contrasts with the generalization capabilities offered by NNs, which can better interpolate or even extrapolate with novel input scenarios. While both NNs and GAMs are capable of predicting spectral content, the flexibility and multi-output nature of NNs streamline the modeling process and provide richer information for sophisticated noise modeling and impact assessments, which are increasingly important for effective management of anthropogenic noise in marine environments (Lee *et al.*, 2021).

While NNs offer powerful predictive capabilities and the advantage of modeling complex, nonlinear relationships across multiple outputs simultaneously, they are not without important limitations. A primary concern with NNs is their limited interpretability. Because they function as "black box" models, the internal reasoning behind their predictions is not always easily accessible or transparent to users (Hassija *et al.*, 2024). This stands in contrast to more interpretable statistical approaches, such as GAMs, where the influence of each predictor can be directly visualized and quantified through model coefficients and smooth functions. Although tools such as partial dependence plots (as shown in Fig. 7) and effect size calculations (as shown in Fig. 8) offer insights into the relationships learned by a NN, these approaches provide only indirect insights and may not capture all aspects of the model's decision-making process (Hassija *et al.*, 2024). This trade-off between predictive power and interpretability necessitates a balanced approach, combining NN efficiency with GAM-like explicability for scenarios requiring regulatory validation or mechanistic understanding. Such complementary frameworks could leverage the strengths of both methodologies, ensuring robust predictions and workflow efficiency while maintaining interpretability.

The consistency in median error across models suggests that six variables—SOG, gross tonnage, deadweight, length, current magnitude, and wind magnitude—are the most influential variables for MSL prediction in our datasets. We included vessel MMSI, ship builder, engine builder, size class, and vessel type as categorical predictors to account for vessel-specific effects not captured by other variables. This allowed us to identify vessels that had consistently higher or lower MSLs than expected based on their other characteristics. However, it is important to note that this categorical predictor only improves predictions for vessels included in the training dataset and does not generalize to new vessels with previously unseen MMSIs, builders, size class, or vessel type. In such cases, the model relies on other

ship characteristics and this parameter provides no predictive benefit. For broader applicability, our model relies on the other predictor variables when encountering previously unmeasured vessels. Other variables, such as year built and draft, contribute to MSL prediction, reducing the error of the model. Future studies would benefit from incorporating real-time load data to provide a more comprehensive understanding of the relationship between vessel loading conditions and MSL, especially considering that the U.S. Gulf Coast exports large quantities of petroleum products, which may impact ship MSLs (EIA, 2024).

The ability to understand and accurately predict ship MSL enables the simulation and comparison of the potential effectiveness of noise reduction strategies. For example, Findlay *et al.* (2023) demonstrated that a 6 dB reduction in MSL achieved by any source level reduction approach (e.g., slow down or technological modification) could reduce the swathe (strip width ensonified as the ship moves through the habitat) by 50% and the instantaneous acoustic footprint by 75%. Vessel speed reduction has been implemented on the U.S. West Coast, U.S. East Coast, and in Canada and South Korea, with programs observing URN reductions ranging from 3 to 6 dB when vessel speeds were lowered by 1–3 kn (Putland *et al.*, 2018; Leaper, 2019; MacGillivray *et al.*, 2019; An *et al.*, 2021; Burnham *et al.*, 2021; ZoBell *et al.*, 2021; Lee *et al.*, 2022). Similarly, vessel speed reduction may be an effective noise reduction strategy in the GOM. Our NN model results suggest that vessels operating at 20 kn slowed to 10 kn would see a 6–8 dB noise reduction and vessels operating at 15 kn slowed to 10 kn would see a 3–4 dB noise reduction. Additionally, technical modifications to vessel design and components like propellers can help lower the overall noise output (Gassmann *et al.*, 2017a; Leaper, 2019; ZoBell *et al.*, 2023). This study suggests that MSL is not determined by speed alone, but rather by other factors, including load metrics (deadweight and gross tonnage) as well as ship type, length, and environmental conditions (Ross, 2005; McKenna *et al.*, 2012). Taking these various elements into account can support the development of accurate noise models and effective noise reduction strategies. By examining the spectral characteristics and broadband levels of the five most common ship types within our dataset, we find that our results align with studies from other regions (MacGillivray *et al.*, 2022; ZoBell *et al.*, 2023; Shajahan *et al.*, 2024), suggesting that the GOM shipping noise profile is not uniquely different from other heavily trafficked areas; however, the unique composition of ships in the GOM necessitates separate study. The consistency across regions implies that vessel noise reduction strategies developed elsewhere could be effectively applied in the GOM while highlighting the potential for GOM-specific data to inform global shipping noise models.

V. CONCLUSION

This study fills a critical knowledge gap by providing MSLs for approximately 1500 tankers, significantly

J. Acoust. Soc. Am. **158** (3), September 2025

Johnson *et al.*   2265

expanding our understanding of tanker MSL in the global merchant fleet. We provide a large dataset in a different geographical context than previous studies by focusing on the GOM, offering unique insights into the MSL characteristics of the Atlantic tanker fleet, and employ advanced modeling techniques, enabling a more robust understanding of tanker MSL variability and its predictors across different operational and environmental conditions. This comprehensive approach represents an important step forward in managing tanker noise in the GOM and potentially in other regions. SOG, gross tonnage, deadweight, length, current magnitude, and wind magnitude were identified as the most influential predictors of MSL within the commercial vessel category (i.e., cargo ships and tankers). Vessel type is also an important predictor when looking at MSL for all ship types. This work has direct implications for noise management strategies in marine environments. For example, vessel slowdowns or retrofitting could be targeted for vessels identified with consistently higher URN levels based on their design or operational parameters. Future research could explore additional predictors such as real-time loading conditions and maintenance status to further refine noise prediction models and mitigation measures.

SUPPLEMENTARY MATERIAL

See the supplementary material for detailed descriptions of passive acoustic monitoring deployment locations, acoustic recording effort, raw and derived ship variables, environmental parameters, monopole source level calculations, vessel draft estimation methods, and comprehensive model summary statistics.

AUTHOR DECLARATIONS
Conflict of Interest

The authors have no conflicts to disclose.

DATA AVAILABILITY

The data that support the findings of this study are available from the corresponding author upon reasonable request.

Ainslie, M. A., Martin, S. B., Trounce, K. B., Hannay, D. E., Eickmeier, J. M., Deveau, T. J., Lucke, K., MacGillivray, A. O., Nolet, V., and Borys, P. (**2022**). "International harmonization of procedures for measuring and analyzing of vessel underwater radiated noise," Mar. Pollut. Bull. **174**, 113124.

An, J., Lee, K., and Park, H. (**2021**). "Effects of a vessel speed reduction program on air quality in port areas: Focusing on the big three ports in South Korea," J. Mar. Sci. Eng. **9**, 407.

Andrew, R. K., Howe, B. M., Mercer, J. A., and Dzieciuch, M. A. (**2002**). "Ocean ambient sound: Comparing the 1960s with the 1990s for a receiver off the California coast," ARLO **3**, 65–70.

Arveson, P. T., and Vendittis, D. J. (**2000**). "Radiated noise characteristics of a modern cargo ship," J. Acoust. Soc. Am. **107**, 118–129.

Audoly, C. D., and Meyer, V. (**2017**). "Measurement of radiated noise from surface ships—Influence of the sea surface reflection coefficient on the Lloyd's mirror effect," in *Proceedings of Acoustics 2017*, Perth, Australia (Australian Acoustical Society, Perth, Australia).

Benkendorf, D. J., and Hawkins, C. P. (**2020**). "Effects of sample size and network depth on a deep learning approach to species distribution modeling," Ecol. Inf. **60**, 101137.

Bureau of Ocean Energy Management and National Oceanic and Atmospheric Administration (**2023**). "AccessAIS—MarineCadastre.gov," https://marinecadastre.gov/accessais/ (Last viewed August 2024).

Burnham, R. E., Vagle, S., O'Neill, C., and Trounce, K. (**2021**). "The efficacy of management measures to reduce vessel noise in critical habitat of southern resident killer whales in the Salish Sea," Front. Mar. Sci. **8**, 664691.

Carey, W. M. (**2009**). "Lloyd's mirror-image interference effects," Acoust. Today **5**(2), 14–20.

Chapman, N. R., and Price, A. (**2011**). "Low frequency deep ocean ambient noise trend in the Northeast Pacific Ocean," J. Acoust. Soc. Am. **129**, EL161–EL165.

Chion, C., Lagrois, D., and Dupras, J. (**2019**). "A meta-analysis to understand the variability in reported source levels of noise radiated by ships from opportunistic studies," Front. Mar. Sci. **6**, 714.

EIA (**2024**). "Petroleum & other liquids," (U.S. Energy Information Administration, Washington, DC), https://www.eia.gov/dnav/pet/hist/LeafHandler.ashx?n=PET&s=MTTEXP31&f=A (Last viewed October 2024).

Estabrook, B. J., Ponirakis, D. W., Clark, C. W., and Rice, A. N. (**2016**). "Widespread spatial and temporal extent of anthropogenic noise across the northeastern Gulf of Mexico shelf ecosystem," Endang. Species Res. **30**, 267–282.

Etter, P. C. (**2018**). *Underwater Acoustic Modeling and Simulation* (CRC Press, Boca Raton, FL).

Findlay, C. R., Rojano-Doñate, L., Tougaard, J., Johnson, M. P., and Madsen, P. T. (**2023**). "Small reductions in cargo vessel speed substantially reduce noise impacts to marine mammals," Sci. Adv. **9**, eadf2987.

Frasier, K. E., Soldevilla, M. S., Kadifa, M. A., Hodge, L., Frouin-Mouy, H., Tenorio-Hallé, L., Debich, A., Pérez Carballo, I., Johnson, K., Barrera Diaz, I. C., Gracia, A., Serrano, A., Garrison, L. P., Hildebrand, J. A., Le Henaff, M., Ortega Ortiz, J., and Wall-Bell, C. (**2023**). "LISTEN GoMex: 2020–2023: Long-term investigations into soundscapes, trends, ecosystems, and noise in the Gulf of Mexico," Marine Physical Laboratory Technical Memorandum 667, Version 1.3 (Scripps Institution of Oceanography, University of California San Diego, La Jolla, CA), p. 127.

Frasier, K. E., ZoBell, V. M., MacGillivray, A. O., Dolman, J. N., Ainsworth, L., and Zhao, J. (**2022**). "Evaluation of ECHO vessel noise correlation models with a novel dataset collected in the Santa Barbara Channel," Marine Physical Laboratory Technical Memorandum 658 (Scripps Institution of Oceanography, University of California, San Diego, La Jolla, CA).

Friedman, J. H. (**2001**). "Greedy function approximation: A gradient boosting machine," Ann. Statist. **29**, 1189–1232.

Fukushima, K. (**1980**). "Neocognitron: A self-organizing neural network model for a mechanism of pattern recognition unaffected by shift in position," Biol. Cybern. **36**, 193–202.

Gao, F., Ma, Y., Zhang, B., and Xian, M. (**2022**). "SepNet: A neural network for directionally correlated data," Neural Netw. **153**, 215–223.

Gassmann, M., Kindberg, L. B., Wiggins, S. M., and Hildebrand, J. A. (**2017a**). "Underwater noise comparison of pre- and post-retrofitted MAERSK G-class container vessels," CA MPL TM-616 (Scripps Institution of Oceanography, University of California San Diego, La Jolla, CA).

Gassmann, M., Wiggins, S. M., and Hildebrand, J. A. (**2017b**). "Deep-water measurements of container ship radiated noise signatures and directionality," J. Acoust. Soc. Am. **142**(3), 1563–1574.

Gray, L. M., and Greeley, D. S. (**1980**). "Source level model for propeller blade rate radiation for the world's merchant fleet," J. Acoust. Soc. Am. **67**, 516–522.

Greenwell, B. M., Boehmke, B. C., and McCarthy, A. J. (**2018**). "A simple and effective model-based variable importance measure," arXiv:1805.04755.

Hassija, V., Chamola, V., Mahapatra, A., Singal, A., Goel, D., Huang, K., Scardapane, S., Spinelli, I., Mahmud, M., and Hussain, A. (**2024**). "Interpreting black-box models: A review on explainable artificial intelligence," Cogn. Comput. **16**, 45–74.

Hastie, T., and Tibshirani, R. (**1986**). "Generalized additive models," Statist. Sci. **1**, 297–310.

Haver, S. M., Adams, J. D., Hatch, L. T., Van Parijs, S. M., Dziak, R. P., Haxel, J., Heppell, S. A., McKenna, M. F., Mellinger, D. K., and Gedamke, J. (**2021**). "Large vessel activity and low-frequency underwater sound benchmarks in United States waters," Front. Mar. Sci. **8**, 669528.

Haver, S. M., Gedamke, J., Hatch, L. T., Dziak, R. P., Van Parijs, S., McKenna, M. F., Barlow, J., Berchok, C., DiDonato, E., Hanson, B., Haxel, J., Holt, M., Lipski, D., Matsumoto, H., Meinig, C., Mellinger, D. K., Moore, S. E., Oleson, E. M., Soldevilla, M. S., and Klinck, H. (**2018**). "Monitoring long-term soundscape trends in U.S. waters: The NOAA/NPS Ocean Noise Reference Station Network," Mar. Policy **90**, 6–13.

Hildebrand, J. A. (**2009**). "Anthropogenic and natural sources of ambient noise in the ocean," Mar. Ecol. Prog. Ser. **395**, 5–20.

Houser, D. S., Gomez-Rubio, A., and Finneran, J. J. (**2008**). "Evoked potential audiometry of 13 Pacific bottlenose dolphins (*Tursiops truncatus gilli*)," Mar. Mammal Sci. **24**, 28–41.

IMO (**2010**). "Noise from commercial shipping and its adverse impacts on marine life. Report of the Correspondence Group presented to IMO Marine Environment Protection Committee (MEPC 61/19)" (International Maritime Organization, London, UK).

IMO (**2023**). "Revised guidelines for the reduction of underwater radiated noise from shipping to address adverse impacts on marine life (MEPC 1/Circ.906)" (International Maritime Organization, London, UK).

ISO (**2019**). ISO 17208-2:2019. "Underwater acoustics—Quantities and procedures for description and measurement of underwater sound form ships" (International Organization for Standardization, Geneva, Switzerland).

Jalkanen, J. P., Johansson, L., Liefvendahl, M., Bensow, R., Sigray, P., Östberg, M., Karasalo, I., Andersson, M., Peltonen, H., and Pajala, J. (**2018**). "Modelling of ships as a source of underwater noise," Ocean Sci. **14**, 1373–1383.

Jensen, F. B., Kuperman, W. A., Porter, M. B., and Schmidt, H. (**2011**). *Computational Ocean Acoustics* (Springer Science & Business Media, Berlin, Germany).

Jenson, J. J. (**2001**). "Hull girder vibrations," in *Load and Global Response of Ships*, Elsevier Ocean Engineering Series (Elsevier, Amsterdam, the Netherlands), Chap. 6, pp. 241–284.

Karasalo, I., Östberg, M., Sigray, P., Jalkanen, J.-P., Johansson, L., Liefvendahl, M., and Bensow, R. (**2017**). "Estimates of source spectra of ships from long term recordings in the Baltic Sea," Front. Mar. Sci. **4**, 164.

Leaper, R. (**2019**). "The role of slower vessel speeds in reducing greenhouse gas emissions, underwater noise and collision risk to whales," Front. Mar. Sci. **6**, 505.

Leaper, R., Renilson, M., and Ryan, C. (**2014**). "Reducing underwater noise from large commercial ships: Current status and future directions," J. Ocean Technol. **9**, 65–83.

Lee, C. K., Samad, M., Hofer, I., Cannesson, M., and Baldi, P. (**2021**). "Development and validation of an interpretable neural network for prediction of postoperative in-hospital mortality," npj Digit. Med. **4**, 8.

Lee, J.-U., Lee, W.-J., Jeong, E.-S., Noh, J.-H., Kim, J.-S., and Lee, J.-W. (**2022**). "Algorithm for monitoring emissions based on actual speed of ships participating in the Korean vessel speed reduction program," Energies **15**, 9555.

Lin, S., Kim, J., Hua, C., Kang, S., and Park, M.-H. (**2023**). "Comparing artificial and deep neural network models for prediction of coagulant amount and settled water turbidity: Lessons learned from big data in water treatment operations," J. Water Process Eng. **54**, 103949.

Liu, C., Zhao, G., Wang, L., Xie, X., Chen, H., Xie, Y., Gao, F., Tang, Y., and Lang, J. (**2025**). "T2TNet: Tree-to-Transformer Neural Network for high-precision prediction of ship machinery noise," in *Proceedings of the 2024 2nd International Conference on Frontiers of Intelligent Manufacturing and Automation*, Baotou, China (Association for Computing Machinery, New York), pp. 472–477.

Louisiana Department of Transportation and Development (**2024**). "Louisiana offshore oil port," http://www.dotd.la.gov/Inside_LaDOTD/Divisions/Multimodal/LOOP/Pages/default.aspx (Last viewed October 2024).

Lucke, K., Popper, A. N., Hawkins, A. D., Akamatsu, T., André, M., Branstetter, B. K., Lammers, M., Radford, C. A., Stansbury, A. L., and Aran Mooney, T. (**2016**). "Auditory sensitivity in aquatic animals," J. Acoust. Soc. Am. **139**, 3097–3101.

MacGillivray, A., and de Jong, C. (**2021**). "A reference spectrum model for estimating source levels of marine shipping based on automated identification system data," J. Mar. Sci. Eng. **9**(4), 369.

MacGillivray, A. O., Ainsworth, L. M., Zhao, J., Dolman, J. N., Hannay, D. E., Frouin-Mouy, H., Trounce, K. B., and White, D. A. (**2022**). "A functional regression analysis of vessel source level measurements from the Enhancing Cetacean Habitat and Observation (ECHO) database," J. Acoust. Soc. Am. **152**, 1547–1563.

MacGillivray, A. O., Li, Z., Hannay, D. E., Trounce, K. B., and Robinson, O. M. (**2019**). "Slowing deep-sea commercial vessels reduces underwater radiated noise," J. Acoust. Soc. Am. **146**, 340–351.

MarineTraffic (**2023**). "MarineTraffic: Global Ship Tracking Intelligence," https://www.marinetraffic.com/ (Last viewed August 2024).

MathWorks (**2023**). "MATLAB version 9.14.0 (R2023a) [computer program]" (MathWorks, Inc., Natick, MA), https://www.mathworks.com (Last viewed June 2025).

McDonald, M. A., Hildebrand, J. A., and Wiggins, S. M. (**2006**). "Increases in deep ocean ambient noise in the Northeast Pacific west of San Nicolas Island, California," J. Acoust. Soc. Am. **120**, 711–718.

McKenna, M. F., Ross, D., Wiggins, S. M., and Hildebrand, J. A. (**2012**). "Underwater radiated noise from modern commercial ships," J. Acoust. Soc. Am. **131**, 92–103.

McKenna, M. F., Wiggins, S. M., and Hildebrand, J. A. (**2013**). "Relationship between container ship underwater noise levels and ship design, operational and oceanographic conditions," Sci. Rep. **3**, 1760.

Meyers, S., Yilmaz, Y., and Luther, M. (**2022**). "Some methods for addressing errors in static AIS data records," Ocean Eng. **264**, 112367.

Miksis-Olds, J. L., and Nichols, S. M. (**2016**). "Is low frequency ocean sound increasing globally?," J. Acoust. Soc. Am. **139**, 501–511.

Naval Research Laboratory (**2014–2024**). "Global Ocean Forecast System (GOFS) 3.1," https://www.hycom.org/dataserver/gofs-3pt1/analysis (Last viewed August 2024).

Peng, C., Zhao, X., and Liu, G. (**2015**). "Noise in the sea and its impacts on marine organisms," Int. J. Environ. Res. Public Health **12**, 12304–12323.

Piccolo, J., Haramuniz, G., and Michalopoulou, Z.-H. (**2019**). "Geoacoustic inversion with generalized additive models," J. Acoust. Soc. Am. **145**, EL463–EL468.

Port of Galveston (**2024**). "Port of Galveston," https://portofgalveston.com/ (Last viewed October 2024).

Port of South Louisiana (**2024**). "Port of South Louisiana," https://portsl.com/facts-at-a-glance/ (Last viewed October 2024).

Putland, R. L., Merchant, N. D., Farcas, A., and Radford, C. A. (**2018**). "Vessel noise cuts down communication space for vocalizing fish and marine mammals," Glob. Change Biol. **24**, 1708–1721.

R Core Team. (**2024**). *R: A Language and Environment for Statistical Computing* (R Foundation for Statistical Computing, Vienna, Austria).

Ross, D. (**1976**). *Mechanics of Underwater Noise* (Pergamon Press, Oxford, UK).

Ross, D. (**2005**). "Ship sources of ambient noise," IEEE J. Ocean. Eng. **30**, 257–261.

Shajahan, N., Halliday, W. D., Dawson, J., Maksagak, I., Weese, K., Melling, H., Niemi, A., Vagle, S., Williams, B., and Insley, S. J. (**2024**). "Opportunistic ship source level measurements in the Western Canadian Arctic," J. Acoust. Soc. Am. **155**, 3807–3821.

Silver, D., Schrittwieser, J., Simonyan, K., Antonoglou, I., Huang, A., Guez, A., Hubert, T., Baker, L., Lai, M., Bolton, A., Chen, Y., Lillicrap, T., Hui, F., Sifre, L., van den Driessche, G., Graepel, T., and Hassabis, D. (**2017**). "Mastering the game of Go without human knowledge," Nature **550**, 354–359.

Szymanski, M. D., Bain, D. E., Kiehl, K., Pennington, S., Wong, S., and Henry, K. R. (**1999**). "Killer whale (*Orcinus orca*) hearing: Auditory brainstem response and behavioral audiograms," J. Acoust. Soc. Am. **106**, 1134–1141.

Texas Comptroller of Public Accounts (**2024**). "Port of Houston," https://comptroller.texas.gov/economy/economic-data/ports/2016/houston.php (Last viewed November 25, 2024).

Tieleman, T., and Hinton, G. (**2012**). "Lecture 6.5—RMSprop: Divide the gradient by a running average of its recent magnitude. Coursera: Neural Networks for Machine Learning at Toronto University." https://www.cs.toronto.edu/~tijmen/csc321/slides/lecture_slides_lec6.pdf (Last viewed January 2025).

Urick, R. J. (**1983**). *Principles of Underwater Sound* (McGraw-Hill, New York).

U.S. Department of Commerce, National Oceanic and Atmospheric Administration, National Ocean Service (**2024**). U.S. Coast Pilot 5, Gulf of Mexico, Puerto Rico, and Virgin Islands, 52nd ed. (NOAA Office of Coast Survey, Silver Spring, MD), Chap. 3.

Veirs, S., Veirs, V., and Wood, J. D. (**2016**). "Ship noise extends to frequencies used for echolocation by endangered killer whales," PeerJ **4**, e1657.

Vorus, W. S. (**2001**). "Ship vibrations," in *Encyclopedia of Vibration*, edited by S. Braun (Elsevier, Oxford, UK), pp. 1167–1173.

Walker, J. L., Zeng, Z., ZoBell, V. M., and Frasier, K. E. (**2024**). "Underwater sound speed profile estimation from vessel traffic recordings and multi-view neural networks," J. Acoust. Soc. Am. **155**, 3015–3026.

Wang, Y., Wang, K., and Abdel-Maksoud, M. (**2021**). "noiseNet: A neural network to predict marine propellers' underwater radiated noise," Ocean Eng. **236**, 109542.

Wiggins, S. M., Hall, J. M., Thayre, B. J., and Hildebrand, J. A. (**2016**). "Gulf of Mexico low-frequency ocean soundscape impacted by airguns," J. Acoust. Soc. Am. **140**, 176–183.

Wiggins, S. M., and Hildebrand, J. A. (**2007**). "High-frequency Acoustic Recording Package (HARP) for broad-band, long-term marine mammal monitoring," in *2007 Symposium on Underwater Technology and Workshop on Scientific Use of Submarine Cables and Related Technologies*, Tokyo, Japan (IEEE, New York), pp. 551–557.

Wilcock, W. S. D., Stafford, K. M., Andrew, R. K., and Odom, R. I. (**2014**). "Sounds in the ocean at 1–100 Hz," Annu. Rev. Mar. Sci. **6**, 117–140.

Wood, S. N. (**2017**). *Generalized Additive Models: An Introduction with R*, 2nd ed. (Chapman and Hall/CRC, London, UK).

ZoBell, V. M., Frasier, K. E., Morten, J. A., Hastings, S. P., Peavey Reeves, L. E., Wiggins, S. M., and Hildebrand, J. A. (**2021**). "Underwater noise mitigation in the Santa Barbara Channel through incentive-based vessel speed reduction," Sci. Rep. **11**, 18391.

ZoBell, V. M., Gassmann, M., Kindberg, L. B., Wiggins, S. M., Hildebrand, J. A., and Frasier, K. E. (**2023**). "Retrofit-induced changes in the radiated noise and monopole source levels of container ships," PLoS One **18**, e0282677.